IEEE Access
Multidisciplinary | Rapid Review | Open Access Journal

Received 7 October 2022, accepted 27 November 2022, date of publication 14 December 2022,
date of current version 20 December 2022.

Digital Object Identifier 10.1109/ACCESS.2022.3229043

SURVEY

Review of Machine Learning Applications to the Modeling and Design Optimization of Switched Reluctance Motors

MOHAMED OMAR[1,2], (Graduate Student Member, IEEE), EHAB SAYED[3], (Member, IEEE), MOHAMED ABDALMAGID[1,2], (Graduate Student Member, IEEE), BERKER BILGIN[1], (Senior Member, IEEE), MOHAMED H. BAKR[1], (Senior Member, IEEE), AND ALI EMADI[1], (Fellow, IEEE)

[1]Department of Electric and Computer Engineering, McMaster University, Hamilton, ON L8S 4S4, Canada
[2]Department of Power Electronics and Energy Conversion Systems, Electronics Research Institute, Cairo 12622, Egypt
[3]Department of Electrical Engineering, Faculty of Engineering at Shoubra, Benha University, Cairo 11629, Egypt

Corresponding author: Mohamed Omar (omarm8@mcmaster.ca)

ABSTRACT This work presents a comprehensive review of the developments in using Machine Learning (ML)-based algorithms for the modeling and design optimization of switched reluctance motors (SRMs). We reviewed Machine Learning-based numerical and analytical approaches used in modeling SRMs. We showed the difference between the supervised, unsupervised and reinforcement learning algorithms. More focus is placed on supervised learning algorithms as they are the most used algorithms in this area. The supervised learning algorithms studied in this work include the feedforward neural networks, recurrent neural networks, support vector machines, extreme learning machines, and Bayesian networks. This work also discusses several essential aspects of the considered machine learning algorithms, such as core concept, structure, and computational time. It also surveys sample data acquisition methods and data size. Finally, comparisons between the different considered ML-based algorithms are conducted in terms of electric motor type, dataset inputs and outputs, and algorithm's structure and accuracy to provide a summary overview of the ML-based algorithms for SRMs modeling and design.

INDEX TERMS Electric machine design, electric machine modeling, machine learning (ML), switched reluctance motor (SRM).

I. INTRODUCTION

Switched reluctance motors (SRMs) are receiving more attention owing to their simple and robust construction, low cost, and fault tolerance capability. SRMs also offer reliable performance and stable operation at high speeds [1], [2]. These advantages make SRMs a promising alternative to conventional electric motors, such as induction motors and permanent magnet synchronous motors (PMSMs). The challenges in SRMs are the high torque ripples, vibration and acoustic noise, and high-level of nonlinearity in modeling. However, extensive research has been conducted to address those issues. SRMs have recently been used in many applications, such as propulsion, machinery, mining, pumps, and domestic appliances [3], [4].

Each application of SRMs requires a set of specific requirements. For example, electric machines in EVs and HEVs should have high torque and power densities, a wide operating speed range, and high efficiency at different operating conditions [5], [6]. Design optimization of SRMs helps significantly in fulfilling these requirements. Design optimization is a multi-objective and nonlinear problem [7]. The design optimization process requires an accurate electromagnetic model that relates the designable parameters to the output objectives [8], [9]. The machine model provides various electromagnetic characteristics such as induced electromotive force, flux density and electromagnetic torque. It also helps calculate the machine losses and assesses the machine performance.

The associate editor coordinating the review of this manuscript and approving it for publication was Mehmet Alper Uslu.

Several nonlinear modeling techniques were developed in the literature. These techniques can be categorized as numerical and analytical techniques. Numerical modeling methods include the finite element analysis (FEA) and the boundary element method (BEM). FEA is one of the widely adopted numerical modeling techniques [10], [11]. Although FEA provides accurate results, it is computationally expensive [12]. On the other hand, the BEM approach has attracted interest in electromagnetic analysis due to its high accuracy and reduced computational burden as compared to FEA [13]. Analytical techniques derive approximate analytical relationships between the designable parameters of the machine and the performance characteristics [14], [15]. The most known analytical modeling methods are based on curve fitting, Maxwell's equations, and magnetic equivalent circuit techniques. Unlike numerical methods, analytical approaches are much less expensive computationally [16]. However, the key challenges of analytical methods are modeling core saturation and end-winding inductance, and calculating eddy current and hysteresis losses [17]. ML-based modeling methods are classified as curve fitting techniques. They became more popular due to the emergence of many advanced AI algorithms. They offer a good generalization capability for modeling nonlinear characteristics. ML-based modeling techniques provide good accuracy at a reasonable computational cost. These techniques are the subject of this paper.

Heuristic and optimization approaches for electric machine design require many simulations to reach an optimal design. ML-based algorithms were recently proposed as surrogate models to reduce the computational cost in FEA [8], [18], [19]. Initially, an FEA model is developed to accurately sample the data space for various combinations of designable parameters. These designable parameters include both geometric and material parameters. ML-based algorithms then model the nonlinear relationship between these parameters and the corresponding output performance characteristics at different operating conditions. This mapping is used as a surrogate model, which significantly decreases the computational time and cost as compared to an FEA model. Finally, a multi-objective optimization algorithm is applied to achieve the optimal design.

This paper discusses various numerical and analytical techniques utilized in the electromagnetic modelling of SRMs. A comprehensive review of ML-based algorithms used for modeling SRMs is presented. This work classifies ML-based algorithms into supervised learning, unsupervised learning, and reinforcement learning. We focus on the supervised learning techniques such as feedforward neural networks, recurrent neural networks, and support vector machines as they are the commonly applied algorithms in the scope of this paper. Moreover, we discuss how these algorithms are adopted for the geometry optimization of SRMs to improve motor performance.

The rest of the paper is organized as follows. Section II discusses the electromagnetic characteristics of SRMs. Section III introduces common numerical and analytical techniques for modeling of SRMs. In Section IV, the classification of ML-based algorithms is presented. Section V reviews ML-based modeling techniques for SRMs. The ML-based surrogates for the modeling and design optimization of SRMs are discussed in Section VI. Potential future work is introduced in Section VII. Finally, concluding remarks are presented in Section VIII.

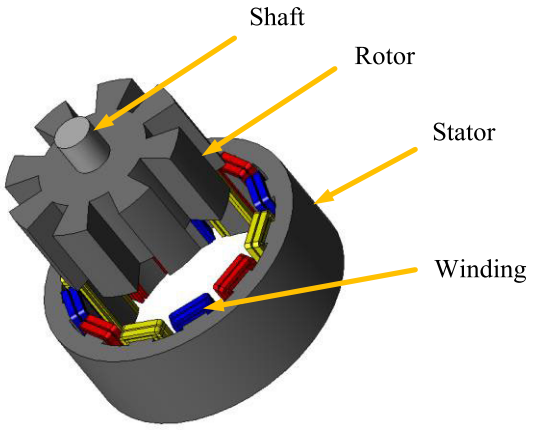

FIGURE 1. A typical structure of a three-phase 12/8 SRM.

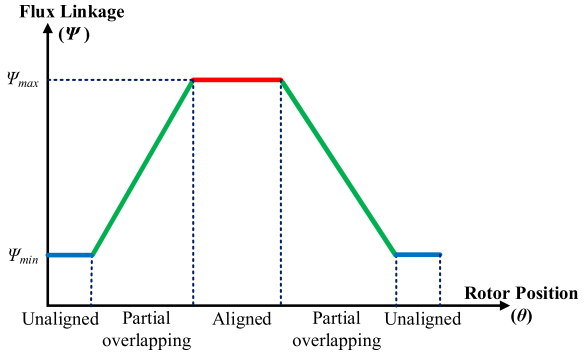

FIGURE 2. Ideal profile of flux linkage versus rotor position.

II. SWITCHED RELUCTANCE MOTORS

SRMs feature a simple and robust construction. Fig. 1 shows a typical structure of a three-phase 12/8 SRM. The stator and rotor consist of a stack of laminated ferromagnetic material. The stator has concentrated windings. The rotor does not have permanent magnets or windings. This makes SRMs easier and less expensive to manufacture with a secure and stable supply chain [20], [21]. Besides, they can run at high temperatures. The SRM phases require independent excitation, which enables programming of the shape of the phase current for performance improvement and fault tolerance capability of the motor drive [22].

On the other hand, the double saliency structure of SRMs brings some challenges, such as high torque ripple, nonlinear magnetic characteristics, and windage losses, especially at high-speed operation. Depending on how the motor is

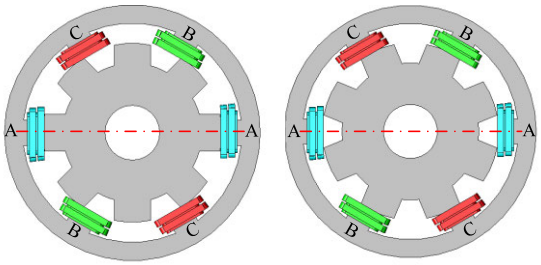

FIGURE 3. Ideal SRM rotor positions with respect to phase A shown on an 6/8 SRM (a) aligned position and (b) unaligned position.

designed and controlled, SRMs might also suffer from lower power density, and torque density compared to PMSMs [23]. Acoustic noise and vibration are the most well-known challenges in SRMs. However, much research has been conducted to tackle these issues and improve motor performance. For example, the authors in [24] proposed a segmental rotor structure to enhance the motor torque density. In [25], the authors used a higher number of rotor poles to improve the torque characteristics. A chamfered rotor poles design has been introduced in [26] to reduce the induced EMF. This led to injecting more current at high speeds and, as a result, improving the torque capability [26]. Also, the acoustic noise and vibration issues have been addressed in [27] by adapting SRM pole configurations and current profiling.

In this paper, we mainly focus on conducting a comprehensive review of the ML-based algorithms applied to modeling and design SRMs. The main goal of modeling SRMs is to determine the relationship between the phase flux linkage ψ, the stator current, i and rotor position,θ [28]. Equations (1)-(3) can be used to get these electromagnetic characteristics. The phase flux linkage is obtained from.

$$\psi(t) = \int_0^t [u(t) - Ri(t)]dt + \psi(0), \tag{1}$$

where $\psi(t)$ is the instantaneous phase flux linkage and $\psi(0)$is the initial flux linkage at $t = 0$. $u(t)$ and $i(t)$ are the instantaneous phase voltage and phase current, respectively, and$R$is the phase resistance.

The electromagnetic torque is directly proportional to the rate of change of co-energy at different rotor positions:

$$T = \left.\frac{\partial W'(i,\theta)}{\partial \theta}\right|_{i=const}, \tag{2}$$

where T is the instantaneous electromagnetic torque, θ is the rotor position, and W' is the co-energy which is given by:

$$W' = \int_0^i \psi(i,\theta)di. \tag{3}$$

An ideal flux linkage profile with respect to rotor position is shown in Fig. 2 for one electrical cycle. There are three central regions based on the rotor position: aligned, partial-overlap and unaligned positions [28]. The SRM rotor pole overlaps the energized stator pole at the aligned position, as depicted in Fig. 3 (a). In contrast, there is no overlap between the stator and rotor poles in the unaligned position, as depicted in Fig. 3 (b). At the unaligned positions, the relative distance between stator and rotor poles is the largest. Thus, the resulting air gap is the largest, and flux linkage is the lowest. In contrast, flux linkage is the highest at the aligned position. The profile of the phase inductance follows an identical pattern to the flux linkage. The inductance rises as the rotor pole moves from unaligned to aligned position. It should be indicated that as the phase current increases, the flux linkage increases. However, at high current levels, the rate-of-change of flux linkage decreases due to the saturation that of the magnetic core [3]. To achieve high torque density, SRMs work in saturation regions [29]. Thus, phase flux linkage exhibits a nonlinear relationship with stator phase current and rotor position [28], [29]. In addition, the airgap periphery is inconsistently distributed due to the salient construction of the stator and rotor poles. These reasons make modeling of SRMs challenging. This motivates research that addresses these issues.

III. MODELING TECHNIQUES FOR SRMs

Undoubtedly, the accurate electromagnetic modeling of SRMs is the basis for design optimization, performance prediction, and current control. Numerous studies have focused on modeling the electromagnetic characteristics of SRMs. These approaches are commonly classified into two main categories: numerical and analytical methods. Fig. 4 summarizes the most common modeling methods for SRMs.

A. NUMERICAL MODELING METHODS

Numerical modeling methods utilized in SRM modeling include FEA and boundary element method (BEM) [30], [31]. FEA is the most common numerical technique. It provides an electromagnetic analysis with high accuracy for motor geometrical parameters. It does not require the assumptions considered in analytical methods [29]. The FEA modeling accuracy is highly dependent on the number of finite elements [32]. Since SRMs commonly operate in the saturated region, a large number of finite elements is required to promote model accuracy [28]. In addition, the airgap of SRMs varies with the rotor operation. This requires a fine mesh close to the airgap. The key disadvantage of FEA modeling is the high computational cost, as one FEA simulation time might extend to hours depending on the model complexity and how fine the utilized mesh is.

BEM is an alternative technique to FEA. It solves the magnetic fields on the boundary domain using the boundary integral equations. It usually requires less computational effort, and its accuracy can be as high as the FEA [33]. However, BEM's main shortcoming is the difficulty of analyzing and solving saturated magnetic fields [30]. To tackle this issue, BEM is usually combined with another modeling method, such as FEA or magnetic equivalent circuit (MEC), to model SRMs [33], [34]. FEA or MEC are used to solve for

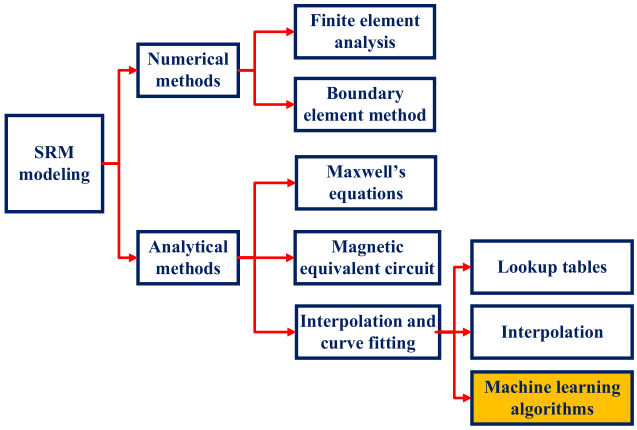

FIGURE 4. Classification of various modeling techniques for SRMs.

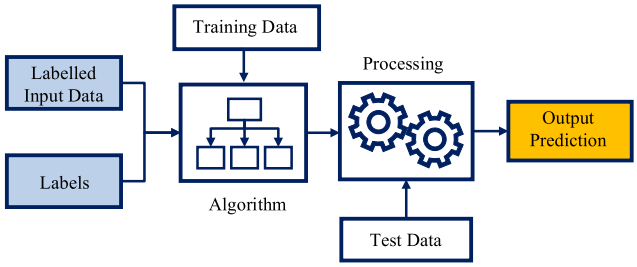

FIGURE 5. The basic flow chart of supervised learning techniques.

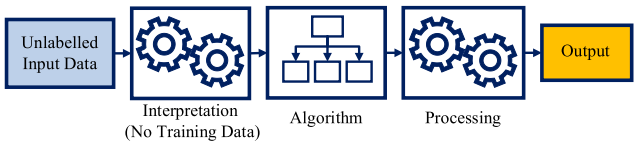

FIGURE 6. The basic flow chart of unsupervised learning techniques.

the electromagnetic fields in the saturated nonlinear regions, while BEM analyzes fields in the linear region.

B. ANALYTICAL MODELING METHODS

Maxwell's equations, magnetic equivalent circuit (MEC), and curve fitting techniques are the most common analytical modeling methods. Maxwell's equations-based models ignore the local saturation, mutual coupling effect, and leakage flux thus limiting the model accuracy [28]. It is commonly preferred in preliminary design stages to determine main design parameters [35], [36].

MEC method is powerful in analyzing and designing electric motors. It develops magnetic circuits for considered machines to study the magnetic characteristics. The MEC method utilizes fewer elements than numerical methods and results in smaller system matrix dimensionality. This provides a significant computation speed [29]. Unlike Maxwell's-based method, MEC method can be improved to consider the magnetic saturation and leakage flux to achieve a closer accuracy with respect to FEA [10]. The magnetic flux path of MEC structures for SRMs should be modified with rotor position. This can be addressed by using empirical formulas or assumptions for the flux paths at various rotor positions based on preceding experience gained from FEA simulations. However, that restricts the generality and accuracy of this method [29].

Curve-fitting models utilize lookup tables, interpolation techniques, or machine learning algorithms to approximate phase flux linkage variation respect to rotor position and stator current [28]. This is achieved based on limited data captured from FEA simulations or experiments.

The look-up table-based method is easy to implement with reasonable accuracy. FEA simulations are used to capture flux linkage, induced voltage and torque characteristics with respect to various stator phase currents and rotor positions. These data are then stored in 2-D (or 3-D when mutual coupling between phases is considered) look-up tables. Then, a dynamic model for the considered SRM is developed solving the time-domain differential equation for the phase current based on the look-up tables. Interpolation is applied to obtain the torque as a function of the rotor position and calculated phase current [37], [38].

Interpolation modeling techniques are used to approximate the nonlinear relationship between the flux linkage or inductance and the phase current by piecewise interpolation functions. For instance, a 2-D bicubic spline and quadratic interpolation function are adopted in [39] and [40] to analyze magnetic performance of SRMs.

ML-based algorithms are used to express the nonlinear nature of the flux linkage, inductance, and torque regarding the SRM phase current and rotor position. The learning algorithms use training datasets acquired through numerical simulations or experiments. The advantage of ML-based algorithms is that they can predict profiles of SRM flux and torque based on limited data. Thus, ML-based techniques reduce required computational efforts as compared to conventional numerical methods [29]. In addition, these techniques are able to adapt to the variation in motor parameters due to losses and manufacturing tolerances [41].

IV. CLASSIFICATION OF MACHINE LEARNING ALGORITHMS

Artificial Intelligence (AI) is a prosperous field with multiple practical applications and active research subjects. ML is the capability of AI systems to derive patterns from raw data to acquire knowledge. ML comprises computational methods that rely on available past information to enhance performance or get accurate predictions. This past information or sample data should be collected carefully since its quality and size are essential for predicting an accurate output [42]. ML-based techniques can provide solutions for many applications such as computer vision, speech recognition, robotics, biology, and medical diagnosis [42]. ML-based algorithms can be classified into supervised, unsupervised, and reinforcement learning [43]. These learning types differ in the sample data and its collection and evaluation.

Supervised learning algorithms are the most utilized ML-based algorithms. They learn from the available examples

(training data) provided by a knowledgeable supervisor. The training data is composed of a set of labelled examples of the input vector and the corresponding output target vector [42]. After training the model, some examples that were not used in the training process are used to test the model's generalization ability. The difference between the predicted and the actual target values determines the prediction error. Fig. 5 illustrates the basic schematic of supervised learning techniques. Supervised learning algorithms are used to address regression and classification problems [42]. Classification is one of the standard learning tasks. Digit and image recognition are examples of classification problems where definite discrete categories are assigned for each input item. The number of categories differs according to the classification problem. Regression is the prediction of a real output value corresponding to a given input vector. An excellent example that explains the difference between the classification and the regression is the weather temperature forecast. A regression model predicts the weather temperature in values such as 20°C. The classification predicts whether the weather is hot or cold. Another regression example related to this work is predicting the torque of an SRM based on the considered motor's flux linkage and current.

In unsupervised learning, the sample data comprises unlabeled examples containing input data without any target vector values [42]. Thus, there is no guide or instructor in this type, and the developed algorithm should learn to use the available data effectively without a guide. Unsupervised learning algorithm can observe the data features. It then attempts to predict the dataset structure, which is known as the probability distribution in the context of machine learning. It can also combine sets of similar examples into homogeneous subsets, known as clustering [42]. A famous clustering example is dividing uncategorized data of two different animals, such as dogs and cats, into two separate clusters. Fig. 6 shows the structure of unsupervised learning techniques. The system does not have any prior knowledge about the features and does not have any dataset for training. The algorithm task is to distinguish the features of the dataset on its own and perform clustering into subsets.

Reinforcement Learning does not have available training examples. Instead, a trial-and-error approach is used to define the training examples. The reinforcement learning approach interacts with the system (simulation model) by receiving observed states and selecting appropriate actions. In response to each control action, the algorithm accepts a feedback signal (reward) taken in each situation [44], as shown in Fig. 7. The reward differentiates between the good and bad action results and defines the objective of the reinforcement learning algorithm. The algorithm tends to maximize the reward over a set of iterations and actions with the system [43].

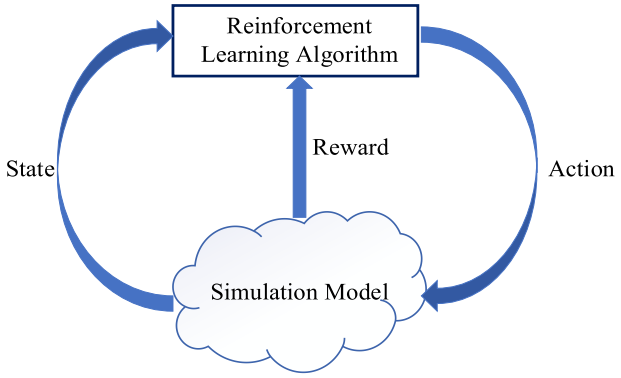

FIGURE 7. The basic flow chart of reinforcement learning technique.

V. MACHINE LEARNING-BASED ALGORITHMS FOR MODELING SRMs

This section presents relevant published work on modeling SRMs using ML-based algorithms. Several algorithms are used for modeling SRMs to accomplish fast computation and accurate results. Almost all machine learning techniques used in this context are supervised learning algorithms. These algorithms include Feedforward Neural Networks (FNN), Recurrent Neural Networks (RNN), Adaptive Neuro-Fuzzy Inference Systems (ANFIS), and Support Vector Machine (SVM).

A. FEEDFORWARD NEURAL NETWORK (FNN)

Artificial Neural Networks (ANNs) have evolved rapidly in recent years due to their capability of learning and generalizing complex relationships, ease of implementation, and fast real-time operation. Feedforward Neural Networks (FNNs) form the basis of several important commercial and industrial applications [45]. An FNN is a mathematical model that approximates functions by mapping features and labels. Features are the attributes associated with each given example. They are defined as the input vector to the learning algorithm. The accurate selection of the features is critical to achieving adequate performance results. This is typically done by the user based on prior knowledge of the learning problem [42]. Labels are the predicted outputs of the algorithm. The label can be a value for a regression problem or a category for a classification task.

Fig. 8 illustrates the basic structure of an FNN with one hidden layer. The information passes forward through the layers of the network. The input vector, X provides initial data, which propagates forward to the computational hidden neurons and finally produces the label, y. The hidden neurons calculate a weighted sum of the features with an added bias, b, as illustrated in (4). This sum then triggers an element-wise nonlinear activation function, $g(z)$. Typically, the hidden neurons are only distinguished from each other by the selection of the type of the activation function.

A recommended default choice for most FNN applications is the rectified linear units (RELU) expressed in (5) [45]. Applying RELU to a linear transformation output produces a nonlinear transformation. The RELU function is a piecewise linear function composed of two linear segments. Therefore, it enables gradient-based optimization and generalization of

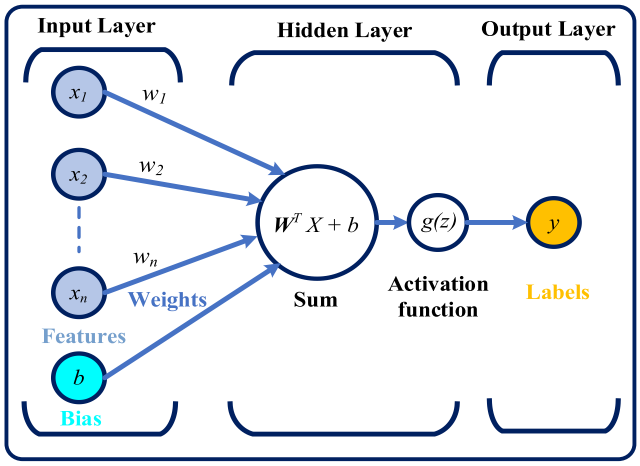

FIGURE 8. The basic structure of FNN with one hidden layer.

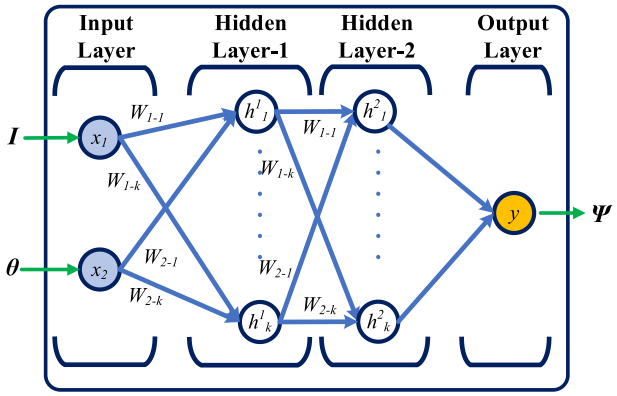

FIGURE 9. The basic structure of FNN with two hidden layers.

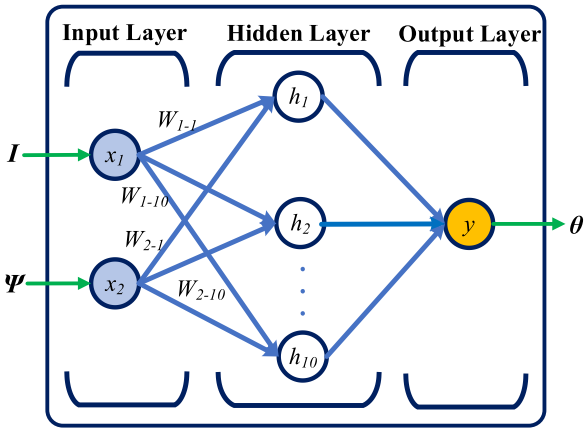

FIGURE 10. The basic structure of a single-layer FNN with ten hidden nodes to model a 6/4 SRM [54].

linear models [45]. Before introducing the RELU activation function, most ANNs used Sigmoid, Hyperbolic Tangent (Tanh), and Tansig functions [45]. These activation functions are expressed in (5). These functions saturate at minimum function output for low stimulus values. They also saturate at maximum output for high stimulus values. They increase

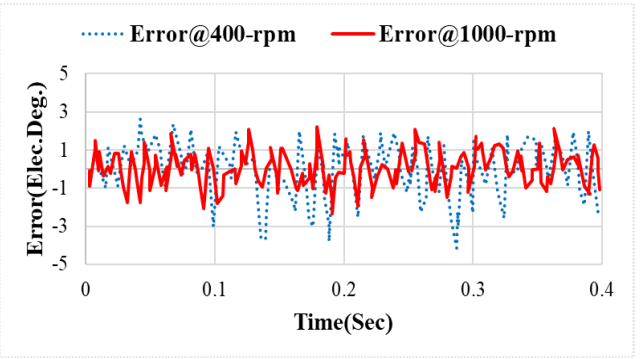

FIGURE 11. Rotor position estimation error profile at 400-rpm and 1000-rpm [54].

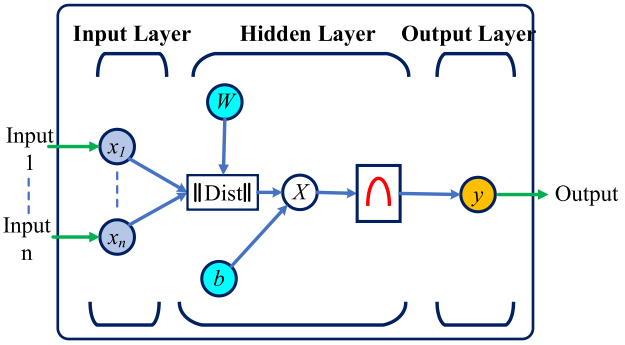

FIGURE 12. A simplified example of RBFNN structure.

monotonically for the values in between the minimum and maximum outputs as the neuron stimulus increases [46].

$$z = W^T X + b \tag{4}$$

$$g(z) = \left\{ \begin{array}{l} \max\{0, z\} - \text{RELU} \\ \dfrac{1}{1+e^{-z}} - \text{Sigmoid} \\ \dfrac{e^z - e^{-z}}{e^z + e^{-z}} - \text{Tanh} \\ \dfrac{1-e^{-2z}}{1+e^{-z}} - \text{Tansig} \end{array} \right\}. \tag{5}$$

The neural network's training process aims at estimating the optimal set of weights, $\boldsymbol{W}$ and optimal bias, b that would achieve the best function approximation. The learning algorithm usually involves an iterative procedure to minimize a loss (error or cost) function, which is used to estimate the algorithm's performance. The loss function is the measurement of the distance between the actual and predicted target response. The prediction error increases as the measured distance increases [45]. The model mean squared error (MSE) is typically used as a loss function to measure the model performance in regression tasks. The ML-based algorithm is then evaluated using a test dataset. The test dataset has not been used during the training process. The main objective of the test dataset is to ensure that the algorithm can generalize the mapping to new input-output pairs.

Due to the FNN's ability to approximate any nonlinear mapping with a certain degree of accuracy, it maintains a high research interest, especially for the multilayer perceptron (MLP) and radial basis function (RBF) networks. MLP is a fully connected FNN which contains one or more hidden layers. The RBF networks are comprised of only a single hidden layer. Backpropagation learning algorithms enable MLP networks to be trained [47]. The following subsections overview the recent literature on using Backpropagation Neural Networks (BPNN) and RBF neural networks in electric motor modeling.

1) BACKPROPAGATION NEURAL NETWORKS (BPNNS)

The backpropagation term describes the training methodology of MLP networks. Standard backpropagation applies gradient descent to the sum-squared error function through two stages. The derivatives of the loss function are evaluated with respect to the neurons' weights. These derivatives are propagated backward through ANN layers. Then, in the second stage, the weights are adjusted based on the evaluated derivatives [43]. The shortcoming of using gradient descent is its slow convergence. In most cases, the gradient descent algorithm (GDA) follows a zigzag pattern to reach an optimal solution, so it might not meet the fast training network requirements [46] [48]. Other gradient-based algorithms can be used to train ANNs, such as conjugate gradient, which searches for an optimal solution along a sequence of conjugate directions. It overcomes issue the GDA has and shows a faster convergence [46]. However, the step size should be adjusted for each iteration, which leads to a computational overhead [48].

Newton's method provides faster convergence than GDA and conjugate gradient approaches. Therefore, it is more favourable, but the high computational cost of calculating the Hessian matrix $\boldsymbol{H}$ (second-order derivatives) is the main concern. Moreover, it does not guarantee a local minimum convergence, especially if the initial point is far from the optimal solution [46]. The quasi-Newton method approximates $\boldsymbol{H}$ with the first-order derivatives. However, it uses a large memory to save the approximate matrix at each training iteration [48].

The Levenberg Marquardt (LM) algorithm tackles the issues with Newton's method. When the sum squared error function is used as a cost function, LM does not require calculating the Hessian matrix. Instead, it uses a Jacobian-based approximation matrix. Generally, LM tends to finish the learning stage in fewer epochs than other discussed algorithms. The number of epochs reflects the number of the total complete passes through the training dataset. It can be adjusted to often hundreds or thousands to allow the learning approach to run until the error is minimized to a sufficient value. Moreover, LM guarantees local minimum convergence. It is evident that Quasi-Newton and LM provide faster convergence at the expense of more memory requirements. LM offers better overall performance as it combines the merits of gradient descent and Newton methods [48]. It is worth noting that the discussed gradient-based approaches obtain a local minimum, which is the global minimum for convex functions. The problem arises if the function is non-convex since it could possibly have multiple local minima [45], [46].

In [49], BPNN was used for modeling a 12/8 1.5-kW SRM. The network structure has one input layer for the two input variables: targeted average torque and rotor position. The BPNN contains two hidden layers with 12 neurons and each neuron utilizes the Hyperbolic Tansig function. However, the output layer utilizes a linear activation function to estimate the output current. An experimental setup was built to collect the training dataset of the torque versus the rotor position at different current levels. The generalization of the learning algorithm is evaluated using a test dataset that was not used during the learning process. The BPNN presented in [49] was applied to control the SRM torque using a torque sharing function (TSF). The TSF is used to determine the desired torque assigned as the network's input. The authors in [49] utilized many numerical optimization algorithms for the network training, such as Quasi-Newton, conjugate gradient, and LM. LM achieved the fastest and the most accurate learning results. The error between the actual (measured) and the predicted output phase current using the LM algorithm was less than 0.1 A.

The authors in [50] used the BPNN structure developed in [49] to provide a model for the torque output of an SRM. This model was utilized in a dynamic control system to minimize the torque ripple. By proposing optimum profiling for the phase current, smooth instantaneous torque waveforms during conduction and commutation periods are obtained. However, no experimental data were presented to validate the simulation results.

A BPNN was also applied in [51] to model an 8/6 SRM. The learning phase of the ANN utilizes 496 measured magnetization data samples. The structure of the BPNN consisted of a single input layer for the current and flux linkage, single hidden layer, and single output layer to estimate the rotor position. The activation function chosen for the hidden layer was a sigmoid, and the output layer was linear. LM managed to finish the training in only 22 epochs with the minimum error compared to conjugate gradient and quasi-Newton algorithms.

Besides BPNN, the authors in [51] developed an SRM model using fuzzy logic (FL) and adaptive neuro-fuzzy inference system (ANFIS) techniques as well. FL is based on the Boolean logic that was first introduced in 1965 [52]. It provides a high level of flexibility to mimic human reasoning based on a predefined set of fuzzy rules. The ANFIS combines the benefits of the FL and ANN [51]. The simulation results manifested that the BPNN had higher accuracy and smaller average percentage error (APE) than FL and ANFIS approaches. The APE of FL and ANFIS was 1.37% and 0.2086%, respectively, whereas that of BPNN was 0.1266%.

The authors in [13] developed real-time modeling of phase inductance and flux linkage of a 4.1-kW 8/6 SRM using FNN. Unlike [51], which used a static locked-rotor test to obtain the

magnetic motor characteristics, this work applied dynamic measurements to achieve an online learning algorithm. The learning process was performed using the BPNN algorithm to optimize the network weights. The network structure is comprised of one input layer assigned for the measured current and rotor position, two hidden layers, and single output layer to estimate the flux linkage, as depicted in Fig. 9. A Gaussian function was utilized as an activation function for both hidden and output layers. The proposed model was validated experimentally. However, as discussed earlier, GDA was applied to train the ANN and optimize the weights, which has a slow convergence.

In [53], two cascaded single-output PBNNs were used for modeling an 8/6 SRM. The first BPNN was used to model the current $i(\psi, \theta)$ and the second for the torque $T(i, \theta)$. The authors used FEA to obtain the dataset. The variation ranges of phase current and rotor position angle used to get the dataset are [0A – 20A] and [0° – 30°], respectively. The chosen step size was 1A for the current and 1° for the rotor position. The training dataset uses even rotor position angles, whereas the test dataset uses the odd ones. The structures of the two BPNNs were similar: single input layer for the inputs, two hidden layers, and single output layer. The total number of hidden neurons to estimate the current and the torque is 10 and 8, respectively. The activation function of the hidden layer was a hyperbolic Tansig, whereas that of the output layer was a linear function.

In [53], LM was utilized as an optimization algorithm for training the network. The mean square error was acted as a loss function for performance evaluation, and the target error was set to 0.0001. The simulation results showed that the generalization capability of the cascaded BPNN models is high. However, the training process took longer time than that in [51]. In [53], It took about 1000 epochs for modeling the current and more than 600 epochs for modeling the torque; however, it took only 22 epochs for modeling the rotor position in [51]. An 8/6 SRM was modelled in both works. That significant difference might be because of the dataset size and the target error used to terminate the learning phase. In fact, the training error, gap between training and test errors, and sample data size should be selected carefully to avoid overfitting and underfitting problems [44]. Overfitting and underfitting are common problems associated with learning in ANNs. Overfitting means that the model is complex and does not fit the new data optimally. It arises when the gap between test and training errors is too large, leading to a significant generalization error. In contrast, underfitting refers to a model that is incapable of fitting the training data with a sufficiently low error value.

The authors in [54] used an FNN to form an efficient mapping for the nonlinear characteristics of an 11.5-kW 6/4 SRM. The current and flux linkage are the inputs to the FNN, and the output is the estimated rotor position, as illustrated in Fig. 10. The training dataset was acquired using two methods. The first uses a suitable magnetization model to calculate flux linkage at random currents and random rotor positions.

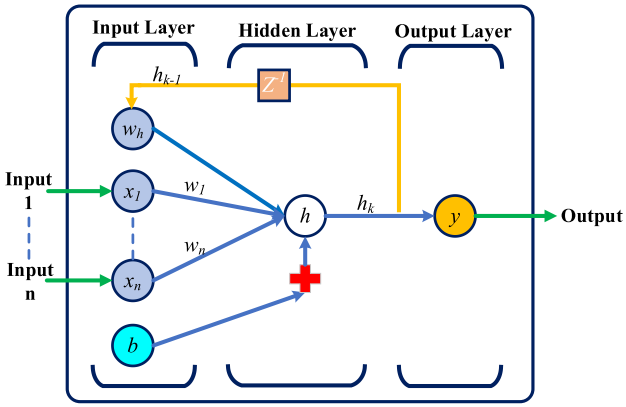

FIGURE 13. A basic structure of RNN.

A detailed study of the magnetization model can be found in [55]. The second method measures the sample data by experimentally measuring phase currents and flux linkages at different rotor positions. The first method was used during the training process, whereas the second one was used during experimental verification.

In [54], a single-layer FNN with ten hidden neurons was proposed to obtain a good balance between the estimated error and the ANN complexity. The hidden layer neurons use sigmoidal activation functions, whereas the output layer utilizes linear transfer function. A test dataset was used to assess the performance and the generalization capability of the learning algorithm. Fig. 11 shows the error between the estimated and real rotor position at 400-rpm and 1000-rpm [54]. It is clear that the error of the rotor position is larger at the lower speed. Thus, the approach presented in [54] introduced an initial approach for a sensorless position estimation for SRM control.

In [56], a BPNN was applied to model the magnetic nonlinearity of SRMs. The flux linkage of the SRM and the position are the inputs to the ANN, whereas the current is the ANN output. Two hidden layers were utilized with hyperbolic tangent transfer functions. The learning algorithm was developed using GDA to adjust the network weights and minimize the error arising from the difference between the actual and predicted outputs. The training dataset was collected experimentally to train the ANN more accurately and efficiently. The training strategy starts with a few hidden neurons. Then the number of the neurons is increased while monitoring the network's generalization capability after each epoch. The generalization capability was evaluated through the testing dataset. The optimal number of hidden neurons was found to be 8 for each hidden layer. The total number of training epochs was 2000. The training results using the BPNN showed great agreement with the experimental outcomes.

In [57], a BPNN was integrated with a genetic algorithm (GA) for modeling a 5.5-kW SRM. GA was applied to obtain a globally optimal solution of the weights, thereby improving the BPNN convergence speed. GA was first used to search a

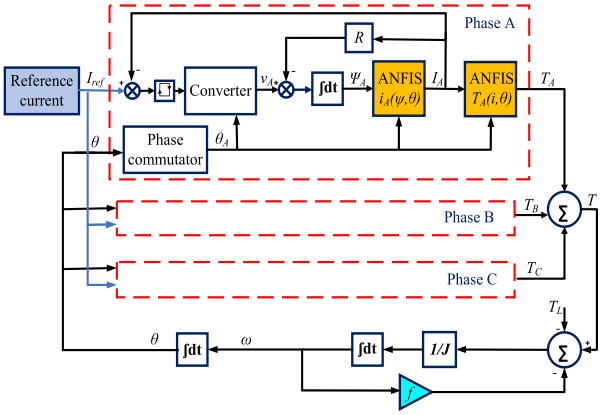

FIGURE 14. The simulation block diagram of a 3-phase SRM using ANFIS to model the torque and flux linkage characteristics [66].

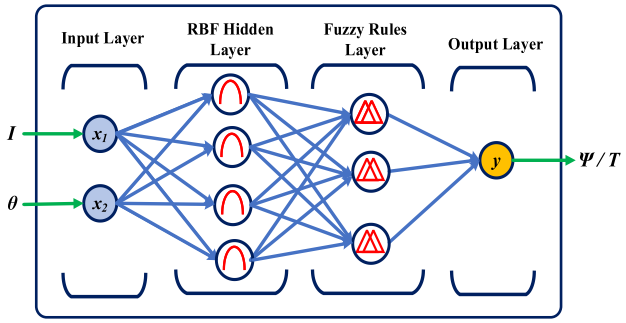

FIGURE 15. The RBFN-AFS architecture proposed in [68] for modeling of torque and flux linkage of an SRM.

definite range in the whole solution space. The BPNN was then applied to find an optimum solution in this specified range. The BPNN is comprised of one hidden layer with 30 neurons, employing a tangent sigmoid activation function, and one output layer with one neuron using a pure linear transfer function. The current and rotor position were assigned as input parameters with the flux linkage as the output response. The training dataset was acquired from static measurements. The flux linkage at various stator currents and rotor positions, obtained from BPNN with GA, was recorded, and it was similar to the static measurements. The authors also verified the GA efficacy by comparing the required number of training steps to those of GDA. Using GA with BPNN reduces the number of epochs to 300 compared to 2000 when GDA is used with BPNN.

2) RADIAL BASIS FUNCTION NEURAL NETWORK (RBFNN)

The structure of the RBF network has only a single hidden layer, as depicted in Fig. 12. The RBF network is considered as a linear function approximator that uses RBFs for its features. Typically, the RBF feature holds a Gaussian response which depends only on the i^{th} measurement of the distance between the central state,$c_i$and the state, Xrelative to the feature width, σ_i [48]:

$$F_i(X) = e^{-\frac{\|X-c_i\|^2}{2\sigma_i^2}}. \tag{6}$$

Some learning techniques for RBF neural networks adjust the centers of the features and the widths as well. The most outstanding merit of RBFNN is that it provides the best approximation along with fast convergence. However, the number of hidden neurons is larger than that used in BPNN [48]. The computational complexity is the downside of RBF networks, especially for nonlinear RBF networks [44]. At the start of the training process, the number of hidden neurons is zero, and it increases gradually until the error difference between the actual and estimated output reaches the target error, or the number of the neurons reaches a prespecified limit.

An RBFNN was used in [58] for modeling the magnetic characteristics of an 8/6 SRM. A set of experimentally measured data for the flux linkage at various stator currents and rotor positions was used for training. The proposed RBFNN is comprised of two inputs for the current and rotor position, six hidden neurons, and one output layer to estimate the flux linkage. The number of epochs for the network training is 100. The simulation outcomes of the proposed RBFNN showed a good match with the experimental training data. However, the authors did not test the generalization ability of the proposed RBFNN using a separate test dataset.

In [48], the authors used an RBFNN and PBNN for modeling a 1.5-kW 12/8 SRM and compared both neural networks. The training dataset was acquired using experimental measurements. The inputs of both neural networks are the flux linkage and stator current, whereas the network output is the position. The structure of the BPNN had a single hidden layer with a Tansig activation function. An LM optimization algorithm was implemented for learning BPNN. The recorded error of the BPNN output (rotor position) was 1.51° when using five hidden neurons. The error increases as the number of neurons decreases. For RBFNN, the optimum number of the hidden neurons was 69, and the maximum rotor position error was 2.07°.

Table 1 compares the two proposed models in terms of MSE, linear regression correlation coefficient (R), and the maximum position error. The minimum the MSE value is, the closer the R value is to 1. R reflects the precision of the test dataset, while the MSE reflects the precision of the training dataset. However, the maximum error indicates the overall model performance because it covers the entire subset of the parameter space [48]. Based on the MSE and R values, the LM-BPNN showed better accuracy than the RBFNN for estimating the rotor position. Experimental verification was carried out for sensorless control of a 12/8 SRM based on the BPNN-developed rotor position. The maximum deviation between the estimated and actual position at low and high speed was less than 4°.

In [59], an RBFNN based on combined clustering was applied to model 0.2-kW 8/6 SRM. The RBFNN is designed by defining the number of hidden neurons and the

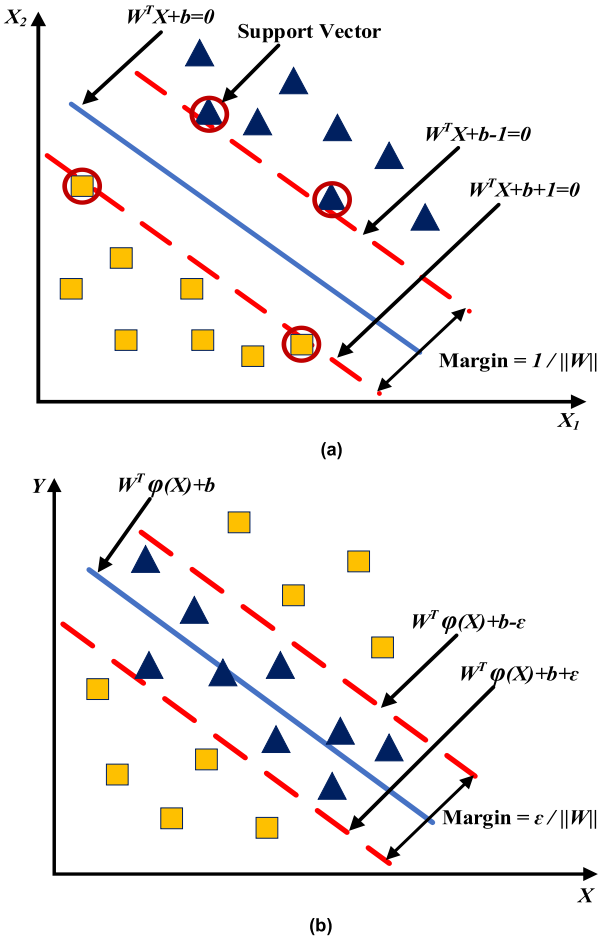

FIGURE 16. The schematic diagram of SVM separating and marginal hyperplanes for the (a) classification and (b) regression tasks. ε in (b) is the tolerable deviation between the hyperplane and the transformed data [69].

TABLE 1. Simulation results of BPNN and RBFNN in [48].

Network style	Number of neurons	MSE	R	Maximum Error
BPNN	5	0.135	0.99821	1.51°
RBFNN	69	0.190	0.997	2.07°

corresponding centers. The design started by determining the center vector using subtractive clustering [59]. Then, the Fuzzy C Mean clustering algorithm was applied to adjust the center points of the network [59]. The training of RBFNN is achieved when the inputs fall close to the center point of the input space. Using FEA, the authors collected the torque and flux linkage training dataset at different currents and rotor positions.

The current and rotor position ranges are [0A – 20A] and [0° – 30°], respectively. The training data of SRM torque was acquired at steps of 1A and 3°, whereas the SRM flux linkage was obtained at steps of 0.4A and 3°. The determined number of hidden neurons is 68, with a learning error of less than 0.001° [59]. After testing the network, a SIMULINK model was established utilizing inversion of the flux linkage look-up table and the torque RBFNNs. The maximum error between the actual rotor position and that obtained using the RBFNN is approximately 6.87° [59]. This work focused on the simulation results, and it did not show the experimental validation. In addition, the number of hidden neurons was quite large, as compared to that of the RBFNN in [48]. This increases the network scale and, hence, increases the computational time for the real-time control.

Apart from the mentioned RBFNN modeling methods in [48], [58], and [59], the authors in [60] introduced a novel way to use some available prior knowledge by using the system boundary value constraints (BVC). Using prior information can help enhance the SRM modeling accuracy and generalization capability. This proposed method is called BVC-RBFNN, and it was applied to model the nonlinear flux linkage characteristics of a 12/8 SRM. The sample dataset was obtained based on a 3D-FEA simulation to consider the end magnetic field effects and provide better calculation results. The stator current and the rotor position are the two inputs used in the proposed BVC-RBFNN. The assigned current range is 0A – 20A, whereas the rotor position range is 0° (unaligned position) - 22.5° (aligned position).

For comparison, the flux linkage characteristics were modeled with the proposed BVC-RBFNN and a conventional RBFNN. The results showed that the BVC-RBFNN demonstrated lower modeling errors. The maximum modeling error using BVC-RBFNN was 83.3% less than the error when using the standard RBFNN. Moreover, A dynamic MATLAB/SIMULINK model was developed using the proposed BVC-RBFNN at 1500 and 3000-rpm. A comparison between the dynamic simulation and experimental results were conducted at the same operating speeds and firing angles to verify the modeling effectiveness of the proposed BVC-RBFNN method. This comparison indicated that the developed BVC-RBFNN-based dynamic simulation model matched well with the experimental outcomes by an estimated error of less than 0.25% for the maximum flux linkage value.

However, the study in [60] did not consider either the effect of using the 3D-FEA model on the modeling precision of SRMs or the simulation time as compared to a 2D-FEA model. Furthermore, the authors in [60] did not consider the simulation time in the provided comparison between the proposed BVC-RBFNN and the conventional RBFNN. Computational cost and accuracy are vital aspects and should both be considered to achieve appropriate modeling.

Similar to [60], the authors in [61] applied BVC-RBFNN for modeling the flux linkage characteristics of an 18.5-kW 12/8 SRM. In [61], online modeling was proposed instead of FEA modeling for training the network. The inputs of the BVC-RBFNN are the phase current [0A – 60A] and rotor position [0° – 22.5°].

The proposed online flux linkage modeling was constructed using an SRM experimental platform that implemented based on digital signal processing (DSP). First, the

real-time sampling phase voltage and current were measured and transmitted using an analog to digital converter (ADC) to be stored in a DSP. Then, the voltage and current data pairs were sent to the computer. Finally, the transmitted data were processed to calculate the flux linkage and form the required input-output training data for the BVC-RBFNN.

The flux linkage results of the proposed method were compared to the conventional RBF, and the error was recorded in terms of the measured flux linkage values. The modeling error of the BVC-RBFNN was less than the conventional RBFNN. Moreover, the authors in [61] compared the BVC-RBFNN training results based on the online modeling and locked rotor test (offline modeling). The results of the online modeling showed higher accuracy, as the relative error was less than 0.01 Wb, representing 0.55% of the maximum flux linkage.

B. RECURRENT NEURAL NETWORK (RNN)

Unlike FNN, Recurrent Neural Network (RNN) utilizes recurrent units that store past information data to handle a sequential input [41], [62]. A neural network is called recurrent when the output or an intermediate state is passed back to the input, thus allowing the use of past data, as shown in Fig. 13.

The authors in [41] adopted a two-layer RNN for parameter identification of an 8/6 SRM. Since the SRM parameters may differ at standstill from dynamic operation due to the losses and saturation, the authors added a parallel damper winding to the magnetization winding to improve the model accuracy. The RNN was adopted to estimate the damper and the magnetizing currents because both are highly nonlinear and not measurable. Besides phase current and rotor position, the phase voltage, v and speed, ω are assigned as inputs to the RNN to consider the motional back EMF. The outputs of the RNN are the magnetization current, I_m and the total phase current (used as a training objective), which are fed back again into the input layer to form RNN.

The chosen activation functions are Tansig for the hidden layer and pure linear for the output layer. After training the RNN using standstill data, the damper current was calculated by subtracting the estimated magnetizing current from the total phase current. The damper voltage was also calculated. As a result, the damper inductance and resistance were identified using the maximum likelihood estimation technique [63]. The proposed online model had been validated, and the results showed its estimation superiority over the standstill model. The average covariance of the phase currents for the online model was 0.6885, whereas that for the standstill model was 0.9127.

C. ADAPTIVE NEURO-FUZZY INFERENCE SYSTEMS (ANFIS)

Adaptive neuro-fuzzy inference system (ANFIS) integrates the expert knowledge of fuzzy logic, represented in membership functions and if-then rules, with the ANN learning power. Thus, it combines the benefits of both FIS and ANN.

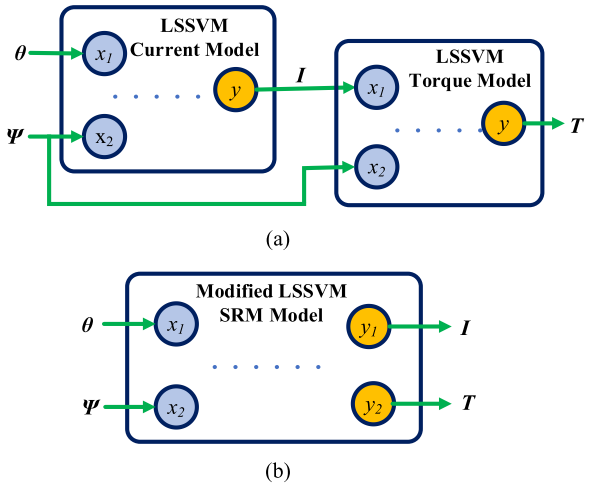

FIGURE 17. LSSVM input-output models (a) cascaded single-output models (b) multi-output model [83].

The ANFIS aims to optimize the FIS parameters using the learning algorithm based on the training data sets. Like ANN, parameter optimization is finished when the error measured between the real and target output is minimized.

In [64], the authors applied an adaptive neuro-fuzzy inference system to identify the inductance of a 6/4 SRM. A hybrid learning technique that combines the backpropagation and least square method was utilized for rapidly training and adapting the fuzzy inference system. The inputs for ANFIS are the stator phase current and rotor position angle, whereas the output is the estimated phase inductance, L. A dataset of 552 samples is generated using FEA; 75% of these data are used for training and 25% for testing ANFIS. The current dataset is between 2A – 24A, whereas the rotor position range is from 0° – 45°. The number of training epochs is 100. The authors assigned 9 Gaussian membership functions for each current and rotor position. Thus, the number of rules is 81. The root mean square errors (RMSEs) for training and testing ANFIS were 1.914e-6 and 3.461e-6, respectively. Thereby, the ANFIS-based inductance profile was in good agreement with that of the FEA model. However, a dynamic simulation and real-time validation need to be investigated. Additionally, a comparison between ANFIS and ANN should be added since the authors in [51] showed that the LM-based BPNN was more accurate than the ANFIS model. ANFIS usually has the potential to converge to a local minimum solution [65].

Another similar approach that uses ANFIS for modeling a 0.55-kW 1500-rpm 6/4 SRM was introduced in [66]. The authors employed ANFIS for modeling the considered SRM flux linkage $\psi(i, \theta)$ and torque $T(i, \theta)$. The flux linkage characteristics were obtained experimentally, and the torque was calculated using the virtual displacement principle [66]. data samples of 396 out of 512 dataset are used for training the network. The remaining sets were used for testing. The RMSE value at the end of the training process was 1.78e-3 Wb for the flux linkage and 0.022 Nm for the torque model. These

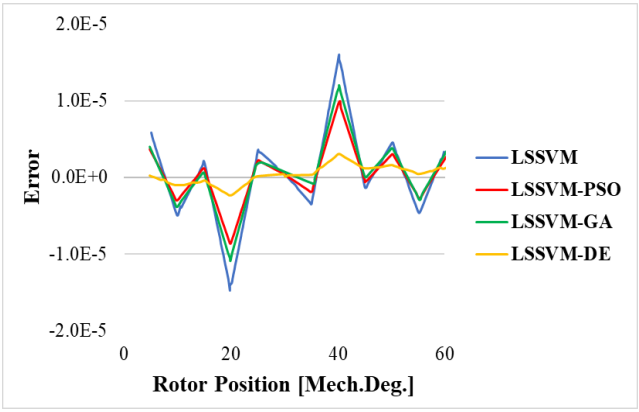

FIGURE 18. Comparison of torque modeling error for LSSVM, LSSVM-GA, LSSVM-PSO and LSSVM-DE [90].

values were reached after 100 epochs. After training ANFIS, the model accuracy was validated by comparing the flux linkage and torque with the corresponding measured data. The authors verified their proposed model by carrying out a dynamic simulation. Fig. 14 shows the block diagram of the SRM dynamic model to simulate its dynamic performance. The maximum deviation in the average torque between the measured and simulated results was less than 10%.

A combination of radial basis function network and an adaptive fuzzy system (RBFN-AFS) was proposed in [67] for modeling and predicting the dynamic performance of a 0.55-kW 1500-rpm 6/4 SRM. The proposed RBFN-AFS comprises four layers, as illustrated in Fig. 15. An input layer transmits the current and rotor position to the hidden layer. A hidden layer uses a Gaussian function as an activation function. The number of hidden neurons is four to obtain an error less than the threshold value. The third layer was dedicated to 64 ($4^3 = 64$) fuzzy rules. Triangular membership functions were adopted for the fuzzy sets. Finally, in the fourth layer, a center of gravity defuzzification approach [67] was employed to calculate the output of the RBFN-AFS. The outputs of the proposed modeling method are flux linkage and torque. The authors in [67] used hierarchically self-organizing learning (HSOL) algorithm to determine the fuzzy rules and adapt the hidden neurons' mean, variance, and weights. This is performed based on the sample data without the need for prior information about the considered motor. The sample data used for training the RBFN-AFS were obtained from measured flux linkage and calculated torque. Two-thirds of the sample data were used for training the neural network, and the remainder was used for testing.

The authors in [67] applied two performance indicators, maximum absolute value of errors (MAVE) and RMSE, to validate the RBFN-AFS accuracy. The flux linkage modeling error represented 0.12% of the maximum flux linkage value, whereas the torque modeling error was 0.22% of the maximum torque value. In addition, the authors compared the BPNN, RBFNN, and the proposed RBFN-AFS methods. The RBFN-AFS showed the highest accuracy and fastest computation. The MAVE of flux linkage and torque of the RBFN-AFS model was less than other methods by at least 84%. Also, the computation time of the RBFN-AFS model was 50% less than that used in BPNN and RBFNN. The proposed modeling method in [67] was implemented in a dynamic simulation and verified experimentally. The dynamic simulation results of RBFN-AFS showed an error of less than 8% compared with the experimental results of the considered SRM prototype.

D. SUPPORT VECTOR MACHINE (SVM)

Support Vector Machine (SVM) is a class of supervised machine learning algorithm that was first presented as a classifier to achieve classification tasks [68]. The Support Vector network nonlinearly maps the input vectors to some high-dimensional feature space. SVM derivation is based on the theory of the statistical learning. SVM can also be used for regression tasks; in this case, it is called a support vector regression (SVR). Fig. 16 (a) shows a schematic diagram of the SVM for the classification tasks. The blue line represents a separating hyperplane that differentiates between two different types of data [69]. The red lines represent the marginal hyperplanes, and the dark red circles located on these planes are called the support vectors. On the other hand, Fig. 16 (b) shows a schematic diagram of the SVM for the regression tasks, which can be used to forecast the data trends. The formula of separating hyperplane is [69]

$$f(X) = W^T \varphi(X) + b, \tag{7}$$

where $\varphi(X)$ denotes the kernel functions that takes the input data X and maps it to high-dimensional solution space.

SVM has gained much popularity since it has overcome ANN problems such as dependency on the size and quality of the sample data, local minima solutions, and the overfitting possibility. SVM has been successfully applied in fault diagnosis [70], [71], speech recognition [72], and data mining [73], [74]. In [75], a combined modeling method for a 1-kW 12/8 SRM using SVM and BPNN was introduced. The flux linkage characteristics were measured without rotor position sensors and clamp devices. Thus, only 64 samples are acquired, which are not sufficient for precise modeling. Therefore, the proposed algorithm in [75] consists of two main steps: data reconstruction and characteristic description. SVM was trained in the data reconstruction stage from the few measured sample data to model the flux linkage characteristics. After that, two BPNNs were adopted in the description stage to model the SRM. One BPNN model is used to model the current $i(\psi, \theta)$ based on the reconstructed data. However, the other BPNN was used to model the torque $T(i, \theta)$ based on the calculated static torque characteristics.

The authors verified the proposed method's accuracy by carrying out dynamic simulation and comparing its results with those from experimental measurements. The discrepancy between the simulation and online estimation of the average torque is 5.7% [75]. The SVM succeeded in converting the flux linkage modeling problem with low-dimensional

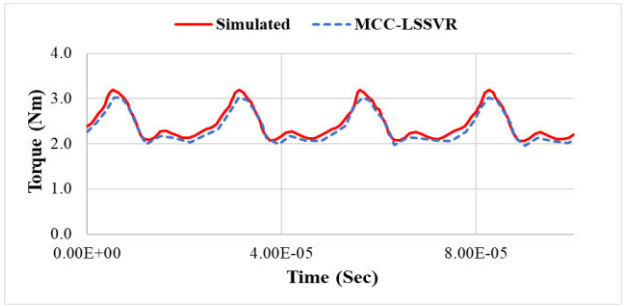

FIGURE 19. Dynamic Torque of MCC-LSSVR model compared to look-up table model at 6000-rpm [91].

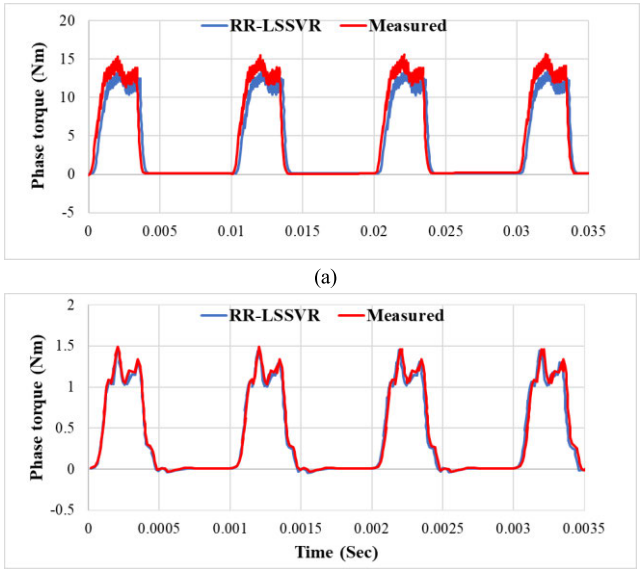

FIGURE 20. Measured and RR-LSSVR Phase torque comparison at (a) 600-rpm and (b) 6000-rpm [65].

space to an optimization problem with a high-dimensional space.

SVM was also formulated to solve nonlinear equations using quadratic programming to avoid local minima solutions. However, this increases the computational burden. In [76], an alternative approach was demonstrated to replace inequality constraints with equality constraints and apply sum squared error (SSE) as a loss function. This approach is known as the least square support vector machine (LSSVM). This reformulation has significantly simplified the problem because the solution became identified by the Karush-Kuhn-Tucker (KKT) linear system [76]. This system can be efficiently solved by utilizing an iterative approach such as the conjugate gradient algorithm. This simplicity makes the LSSVM algorithm faster than standard SVM with less computational time [74], [77]. Similar to SVM, LSSVM can be employed for regression and classification tasks, but its regression model accuracy relies on the values of the hyper-parameters [78].

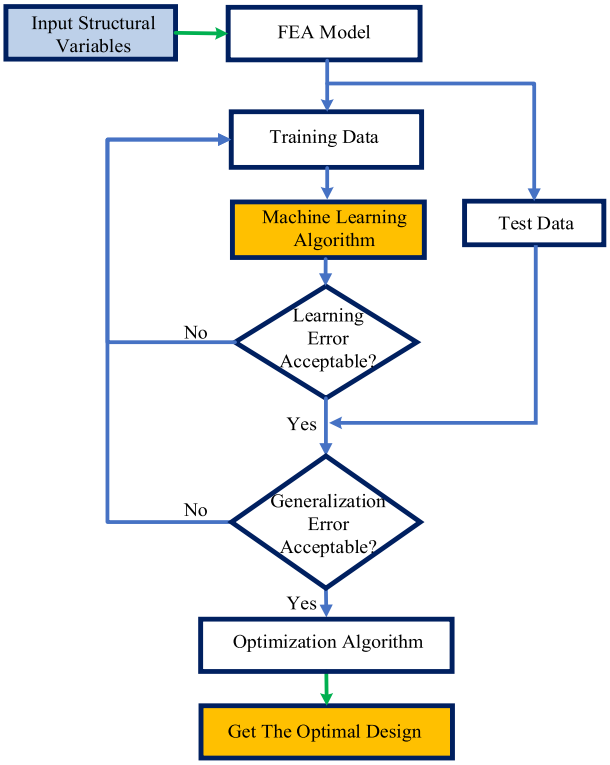

FIGURE 21. A flowchart of motor design optimization using ML-based algorithms.

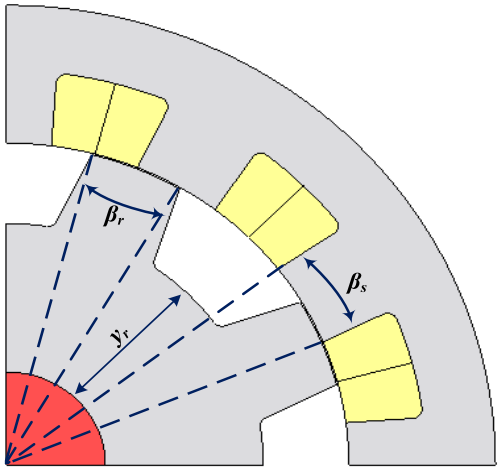

FIGURE 22. A quarter model of the considered SRM showing the stator and rotor arc angles.

Kernel functions are used in LSSVM to map the input data to a higher-dimensional space. There are different kernel functions, such as sigmoid, polynomial, Gaussian, and RBF. The proper selection of the kernel type is essential because this choice affects the LSSVM performance. Moreover, the choice of the regularization, C and kernel width, σ^2 parameters determine the accuracy and the generalization capability. Parameter optimization is thus crucial to obtain

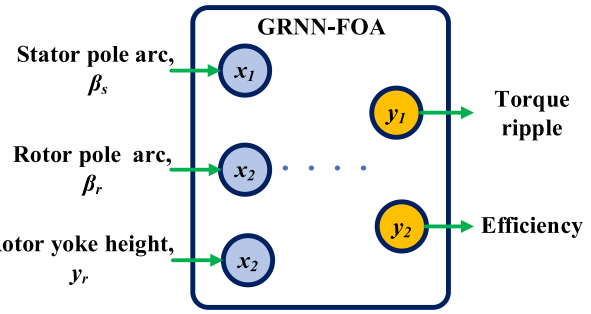

FIGURE 23. The GRNN Input-output modeling system proposed in [102].

optimal performance. The cross-validation (CV) optimization method is usually applied in standard LSSVM. However, the unreasonable prediction accuracy and the relatively long computational time limit its use [79]. Therefore, several optimization algorithms such as Genetic Algorithm (GA), Particle Swarm Optimization (PSO), Artificial Bee Colony (ABC), and Differential Evolution (DE) have been proposed for hyperparameter optimization [80], [81], [82], [83], [84], [85], [86], [87], [88], [89], [90], [91].

In [80], an adaptive genetic algorithm was employed to update the LSSVM parameters. The authors used RBF to be the kernel function of the LSSVM, and the values of the parameters C and σ^2 were obtained using GA. This optimized LSSVM was used to form an efficient mapping structure for modeling nonlinear flux linkage characteristics of a 15-kW 12/8 SRM. The training data set was collected experimentally. The current [0A – 100A] and rotor position [0° – 22.5°] are the inputs to the LSSVM. The total number of the captured training data was 612, whereas the total number of test data was 126. The optimal values of C and σ^2 were 849.17 and 0.0257, respectively. These values were obtained after 12 generations. The GA reduces the training time from 16 minutes when using a CV to 5 min. For validation, the forecasted data were compared with the measured data, and the maximum mean average percentage error (MAPE) value was 0.00782%, which indicates an acceptable generalization performance.

Another LSSVM work was proposed in [81], where a grid diamond search (GDS) was employed to define the kernel function and the regularization parameters. GDS is based on the grid search and diamond search methods. The grid search is applied first to speed up the search and identify the optimal space. The diamond searching algorithm then estimates the optimal solution in the best solution space. Although GDS has an extensive search range and fast convergence, it lacks relative search precision. The recorded computation time of GDS is 6 seconds, but it was 13 minutes for the CV method. The researchers in [81] used the proposed LSSVM-GDS to model the nonlinear characteristics of the flux linkage of an 8/6 SRM. Similar to [80], the rotor position and stator current are taken as inputs. Their corresponding intervals are [0° – 55°] and [0A – 14A], respectively. The proposed model was verified by comparing the forecasted results with the measured data, which reflected satisfactory matching.

Another similar approach based on LSSVM was presented in [82]. A PSO was used to optimize the LSSVM hyperparameters. The proposed LSSVM-PSO was used to model the inductance of a 1-kW 12/8 SRM. The training data set was obtained from a 3D FEA model of the considered SRM. The chosen kernel function in this work is RBF, and PSO optimized the parameters as $C = 124$ and $\sigma^2 = 6.16$. The mean relative error (MRE) of the proposed LSSVM-PSO model was 0.031%, and that of the LSSVM model was 0.068%, which verified the improved accuracy of the proposed model.

An improved 0.5-kW 12/8 SRM model based on LSSVM was introduced in [83]. Two cascaded single-output SRM models were replaced by a multi-output LSSVM to modify the model structure, as shown in Fig. 17. The model inputs are flux linkage and rotor position, whereas the outputs are the phase current and torque. A combination of the RBF and poly kernel functions has been used to enhance the performance of the kernel functions. The parameters of the improved kernel functions were optimized using the CV optimization method. The MSE of the output torque in the test set based on the multi-output LSSVM model is 32.76% of that of the cascaded single model.

An experimental DC-pulse test was performed to obtain 1196 sample data set. The current and rotor position ranges were [1A – 91A] and [−22.5° – 0°], respectively. The data set was split into 728 data pairs for training the LSSVM model and 468 for testing the model performance. The provided simulation results of the modified LSSVM model in [83] showed a decrease in the training time from 4.7 seconds to 2.619 seconds. Also, a noticeable improvement in the phase current model was demonstrated as the error reduced by 3%.

LSSVM lacks sparseness as compared to SVMs because all the dataset points in LSSVM become support vectors [84]. Lack of sparseness increases training time and decreases algorithm prediction accuracy [85]. Sparsity requires less time for out-of-sample extensions because it has fewer support vectors [84]. Therefore, sparse LSSVM was proposed to add sparseness to LSSVMs [86].

The authors in [87] used sparse LSSVM to model nonlinear characteristics of the inverse force function for a planar SRM (PSRM). The inverse force function provides a vital current command for PSRM precise motion. The function is highly nonlinear and limits the accuracy of the model. The training data was acquired from experimental measurements. The dataset is composed of 500 points, 350 points for training and 150 points for testing. The least essential data points of the training set were omitted, and the LSSVM was retrained with the survival points to achieve sparseness.

In [88], RBF was used as the kernel function. The traditional CV method was applied to tune the kernel and regularization parameters. The optimal values of these hyperparameters are $C = 150$ and $\sigma = 0.03$. The calculated RMSE of the training and testing data were 0.3269A and 0.6266A, respectively. The inverse force function modeling results

showed small training and testing errors when the estimated phase current is more than 1A.

The authors in [88] have employed LSSVM with Artificial Bee Colony (ABC) to model flux linkage characteristics of a 0.5-kW 4000-rpm 8/6 SRM. ABC is a meta-heuristic optimization algorithm that mimics the foraging behaviour of a bee swarm [89]. ABC was used in this work to tune the LSSVM hyperparameters. The sample data were obtained using a 2D FEA model. The current and rotor position resemble the model inputs with ranges [0A – 5A] and [31° – 60°], respectively. The training sample size is 450 data pairs, and the testing size is 154.

The regression efficiency of the proposed LSSVM-ABC model [88] was verified against other models such as LSSVM, LSSVM-GA, LSSVM-PSO, and LSSVM-DE, as presented in Table 2. The LSSVM-ABC model offered the best modeling results, with a mean absolute error (MAE) of 0.066%. The minimum fitness value has been achieved after 11 iterations, and the values of the optimal hyperparameters are $C = 3545.88$ and $\sigma^2 = 0.04512$. Although this paper provided a comprehensive comparison between different prediction algorithms, it did not verify the proposed model performance dynamically or experimentally.

The authors in [90] used LSSVM for modeling an 0.5-kW 8/6 SRM. They proposed LSSVM-DE to model the motor torque. The training data was also collected using FEA, where the rotor position range is [0° – 60°] with a step of 1°, whereas the excitation current range is [0A – 3A] with a 0.25A step. The number of data samples captured for training the algorithm is 732, and the test sample uses 144 sample data. In this paper, DE was chosen to optimize C and σ^2 parameters to accomplish the learning and training processes of the selected kernel function. RMSE was assigned as the optimization fitness function to measure learning system accuracy and evaluate the LSSVM performance. Moreover, some statistics metrics were employed as performance indicators, such as MAE, MAPE, and Normalized Mean Square Error (NMSE).

The authors in [90] also conducted a comparison between 6 kernel functions to build the LSSVM. The exponential RBF showed its superiority in terms of the minimum RMSE, as shown in Table 3. Therefore, the exponential RBF was selected to build the LSSVM-DE and validate its regression capability by comparing it with LSSVM, LSSVM-GA, and LSSVM-PSO. The modeling error of the SRM torque profile based on FEA (dataset) and the four algorithms have been shown in Fig. 18 [90]. It is evident that the proposed LSSVM-DE offered the most accurate regression model. Furthermore, the authors carried out a dynamic MATLAB simulation with the proposed LSSVM-DE-based model using the torque and current models. The behaviour of the proposed model imitated that of the FEA-based model.

Although the provided LSSVM algorithms in the earlier mentioned papers [80], [81], [82], [83], [84], [85], [86], [87], [88], [89], [90] were efficient and precise, a potential downside is that the solution might deviate from the inlier samples if outliers existed. The inlier samples denote the samples close to the most normal samples. On the other hand, the outliers represent the samples noticeably far from the remaining samples. To tackle outliers' interference and significant noise problems, an adaptive version of LSSVM is required to assign smaller weights to the outliers with significant errors.

TABLE 2. Comparison of optimized hyperparameters and their correspondence performance indicators for various models [88].

Prediction model	Kernel parameter σ^2	Regularization parameter C	Normalized mean square error NMSE	Mean absolute error MAE [%]
LSSVM	0.0589	3173.08	2.337e-5	0.082
LSSVM-GA	0.04835	3384.71	1.885e-5	0.070
LSSVM-PSO	0.04796	3534.92	1.857e-5	0.069
LSSVM-DE	0.04591	3539.63	1.774e-5	0.067
LSSVM-ABC	0.04512	3543.88	1.741e-5	0.066

TABLE 3. Optimal regularization and kernel functions parameters [90].

Kernel function type	Kernel parameter σ^2	Regularization parameter C	RMSE
Gaussian	0.005306	15,161.35	6.20e-5
RBF	0.005415	16,960.77	6.00e-5
Exponential RBF	0.003407	16,818.16	3.89e-5
Morlet	0.005426	13,840.09	7.39e-5
Mexican Hat	0.005443	14,385.27	7.22e-5
Meyer	σ =0.0742	16,493.5	6.62e-5

In [91], a maximum-correntropy-criterion-based least squares support vector regression (MCC-LSSVR) algorithm was proposed to model the nonlinearity of the flux linkage and torque characteristics of a 1.8-kW 16/10 6000-rpm segmented-rotor SRM (SSRM). Correntropy measures the local similarity between any two arbitrary variables. It was applied as a cost function instead of the conventional SSE method. An FEA model was established to collect the sample data required for training the MCC-LSSVR. The Gaussian function was selected to be the kernel function. Grey Wolf Optimization Algorithm (GWOA) [92] was utilized to tune the hyperparameters of the proposed MCC-LSSVR.

The authors in [91] conducted comparisons with other regression algorithms, like RBFN-AFS, SVM, and LSSVM. MAE and RMSE of the flux linkage and torque modeling showed minimal values when using the MCC-LSSVR. For example, the MCC-LSSVR model reduced the MAE of flux linkage and average torque by 80% and 52%, respectively as compared to the LSSVR. Additionally, dynamic simulations and experimental measurements were carried out at low and high speeds, which validated the effectiveness of the proposed model. For example, the dynamic torque of the MCC-LSSVR model at high speed (6000-rpm) compared to the look-up table model is shown in Fig. 19 [91]. The only disadvantage is

that the nonlinear kernel function in correntropy is commonly restricted to a Gaussian function with a zero-located center. This zero-mean Gaussian function might not be an adequate choice for multiple practical applications [93].

The authors of [91] have also developed recursive robust least squares support vector regression (RR-LSSVR) to regress nonlinear characteristics of the same 16/10 SSRM in [65]. RR-LSSVM was employed to obtain adaptive weights to improve the estimation behaviour with the existence of outliers. The proposed RR-LSSVM uses MCC as the cost function instead of SSE. The SSRM inductance and torque sample data were acquired from experimental measurement instead of FEA to improve the data reliability. PSO was adopted to optimize the RR-LSSVR hyperparameters.

To evaluate the model accuracy and computation time, the RR-LSSVR was compared with BSNN, ANFIS, SVM, and LSSVR. The RR-LSSVR recorded the minimum modeling error and computation time. RR-LSSVR model reduced MAE of inductance and average torque by at least 72% and 67%, respectively, as compared to other methods [65]. It also reduced simulation times by 50%. In addition, simulation and experimental outcomes have validated the effectiveness of the presented approach, which was tested at different speeds. For instance, Fig. 20 shows the compared results of the phase torque between the measured and RR-LSSVR models at 600-rpm and 6000-rpm [65].

A fair comparison of ML-based algorithms used in modeling or designing motors requires some essential aspects, such as similar datasets and similar training techniques with the same trainable hyperparameters [94]. It should also consider the same motor type since many factors can change for different motors. Therefore, it is suggested that new studies in the same field share the captured datasets to help assess future works. Tables 4 and 5 summarize the motor modeling methods considered in this paper using the ANN and SVM algorithms, respectively.

VI. MACHINE LEARNING-BASED ALGORITHMS FOR SRM DESIGN OPTIMIZATION

The design optimization of electric machines is a nonlinear multi-objective problem [7]. It requires repeated calls to the electromagnetic solver. Repeatedly invoking FEA within an optimization loop can be prohibitive. To reduce the computational time of the optimization problems, different surrogate models have been introduced in the literature. Space Mapping (SM) aims at utilizing a fast ''coarse'' model with reduced accuracy [95] to design an accurate but time-intensive ''fine'' model. SM was proposed in [96] to design a brushless DC motor. A kriging surrogate model was used with an evolutionary algorithm to optimize a three-phase PMSM in [97]. Researchers have recently used ML-based algorithms as surrogate models due to their high accuracy and effective generalization ability as compared to other models.

Fig. 21 illustrates a motor design optimization methodology using ML. At the beginning, an initial FEA model is developed to create a reasonable dataset with various combinations of motor geometric parameters. An ML-based technique is then trained using this dataset to map out the nonlinear relationships between the geometric input parameters and corresponding objectives at different operating conditions. The ML-based algorithm provides a good surrogate model of the computationally-expensive FEA. Finally, a multi-objective optimization algorithm is applied to get the optimal design. The surrogate ANN is repeatedly invoked by the optimization algorithm to guide the optimization iterates.

An SRM design process might not be straightforward due to its high nonlinearity. Multiple geometric design parameters should be optimally chosen to fulfill the requirements of the application. These parameters include the number of stator and rotor poles, bore diameter, pole arc angles, taper angles, air gap length, etc. The authors in [98] focused on designing the stator pole arc angle β_s and rotor pole arc angle β_r, shown in Fig. 22, due to their direct impact on the inductance and torque profile.

In [98], a generalized regression neural network (GRNN) was employed in the design procedure of a 3-phase 12/8 SRM. GRNN is a class of probabilistic ANN with a simple structure and fast convergence [99]. It has a better generalization ability than BPNN, especially with a relatively small training dataset, and its output does not converge to the local minima. Additionally, GRNN does not use an iterative process, leading to an incomparably short training time [100]. GRNN has similarities with the RBF method [96], as it has an RBF layer in its structure and a special linear layer. Furthermore, GRNN has only one adjustable parameter known as the spread parameter. This parameter controls the GRNN generalization capability. It should be carefully optimized to enhance the prediction of the motor performance.

The authors in [98] used FEA to obtain static torque characteristics of the considered motor. These data were then used to train an ANN to approximate the objective function. The trained ANN is used as a surrogate to carry out the optimization procedure. The constraints on the pole arc angles in this study were selected to guarantee a fully unaligned position and ensure self-starting capability [101]. In addition, β_s (see Fig. 22) was chosen smaller than β_r to slightly increase copper winding area and aligned/unaligned inductance ratio.

The static torque characteristics were collected for 35 various combinations of both β_s and β_r considering the above constraints [98]. A dynamic model was built based on the static characteristics to get the average torque and the torque ripples. A GRNN is trained to fit input data with specific label data. The trained GRNN is then validated using test data. In [98], An optimization algorithm that exploits GRNN as a surrogate was applied to get the optimal combination of $\beta_s$and β_r to maximize the torque and minimize the torque ripples. The torque ripple was reduced by 12% as compared to the initial design. The proposed method was validated by simulating the optimal geometry using FEA, and the output results were in good agreement with the results of the proposed approach.

In [102], another work using GRNN was proposed for the modeling a 4-kW 12/8 SRM. The model represents the

TABLE 4. Motor modeling methods using NN.

Ref.	Motor	ML-based algorithms	Output (input)	No. of hidden layers / neurons	Activation function of hidden/ output layers	Dataset acquisition method / size	Error
[49]	12/8 SRM	LM-BPNN	$i(T,\theta)$	2/6	Tansig/ pure line	Measured	Error < 0.1 A
[51]	8/6 SRM	LM-BPNN	$\theta(i,\psi)$	1/80	Sigmoid/ pure line	Measured / 496	APE =0.1266%
[13]	8/6 SRM	GDA-BPNN	$\psi(i,\theta)$	2/-	Gauss/ gauss	Online measured	--
[53]	8/6 SRM	LM-BPNN	$i(\psi,\theta)$ & $T(i,\theta)$	2/10	Tansig/ pure line	2D-FEA / 620	Target MSE=0.0001.
[54]	6/4 SRM	FNN	$\theta(i,\psi)$	1/10	Sigmoid/ pure line	[55] / 1000	Error [-5° – +5°]
[56]	SRM	GDA-BPNN	$i(\psi,\theta)$	2/8	Tangent/ pure line	Measured	--
[57]	12/4 SRM	GA-BPNN	$\psi(i,\theta)$	1/30	Sigmoid/ pure line	Measured / 60	Target MSE=0.001
[48]	12/8 SRM	LM-BPNN	$\theta(i,\psi)$	1/5	Tansig	Measured	MSE=0.135 (1.51°)
[48]	12/8 SRM	RBFNN	$\theta(i,\psi)$	1/69	Gauss	Measured	MSE=0.19 (2.07°)
[58]	8/6 SRM	RBFNN	$\psi(i,\theta)$	1/6	Gauss	Measured /120	--
[59]	8/6 SRM	RBFNN	$\psi(i,\theta)$ & $T(i,\theta)$	1/68	Gauss	2D FEA / 500	MSE= 0.0038 (6.87°)
[60]	12/8 SRM	BVC-RBFNN	$\psi(i,\theta)$	--	RBF	3D FEA / 336	Max. error ≈0.5e-4 Wb
[61]	12/8 SRM	BVC-RBFNN	$\psi(i,\theta)$	--	RBF	Online measured	Error <0.01 Wb
[41]	8/6 SRM	RNN	$(i,I_m)(i,\theta,v,\omega)$	--	Tansig/ pure line	Measured/800	Average covariance = 0.9127
[64]	6/4 SRM	ANFIS	$L(i,\theta)$	2/-	Gauss membership	2D FEA / 552	RMSE=3.461e-6
[66]	6/4 SRM	ANFIS	$\psi(i,\theta)$ & $T(i,\theta)$	2/-	Gauss membership	Measured / 512	RMSE=1.78e-3 Wb & 0.022 Nm
[67]	6/4 SRM	RBFN-AFS	$\psi(i,\theta)$ & $T(i,\theta)$	2/4	Triangular membership	Measured / 400	RMSE= 0.35e-3 Wb & 0.0046 Nm

TABLE 5. Motor modeling methods using SVM.

Ref	SRM	ML-based Algorithm	Output(input)	Kernel function	Dataset acquisition method / size	Computation time (Sec)	Error
[75]	12/8	SVM-CV	$\psi(i,\theta)$	RBF	Measured / 64	--	--
[80]	12/8	LSSVM-GA	$\psi(i,\theta)$	RBF	Measured / 738	300	MAPE =0.0078%
[81]	8/6	LSSVM-GDS	$\psi(i,\theta)$	RBF	--	6	--
[82]	12/8	LSSVM-PSO	$L(i,\theta)$	RBF	3D FEA	--	MRE=0.031%
[83]	12/8	LSSVM-CV	$i(\psi,\theta)$ & $T(i,\theta)$	RBF-poly	Measured / 1196	2.619	MSE = 1.487e-3 A & 5.560e-5 Nm
[87]	PSRM	LSSVM-CV	$F(i,x)$	RBF	Measured / 500	--	RMSE= 0.6266 A
[88]	8/6	LSSVM-ABC	$\psi(i,\theta)$	RBF	2D-FEA / 604	--	MAE = 0.066 % MRE=0.38e-3 %
[90]	8/6	LSSVM-DE	$T(i,\theta)$	Exponential RBF	2D-FEA / 876	--	MAE=2.78e-5 % RMSE=3.89e-5%
[91]	16/10 SSRM	MCC-LSSVR-GWOA	$\psi(i,\theta)$ & $T(i,\theta)$	Gaussian	2D-FEA / 350	2.4 & 3.6	RMSE=0.073m Wb & 0.0189 Nm
[65]	16/10 SSRM	RR-LSSVM-PSO	$L(i,\theta)$ & $T(i,\theta)$	Gaussian	Measured	3.3 & 4.1	RMSE =0.0189 mH & 0.0217 Nm

nonlinear relationship of the ripples and operation efficiency with three geometric variables:β_s, β_r and rotor yoke thickness, y_r (see Fig. 23). The spread parameter was optimized using the fruit fly optimization algorithm (FOA), which is based on the foraging pattern of the fruit fly swarm [102]. FEA was used to capture a dataset of 105 samples for

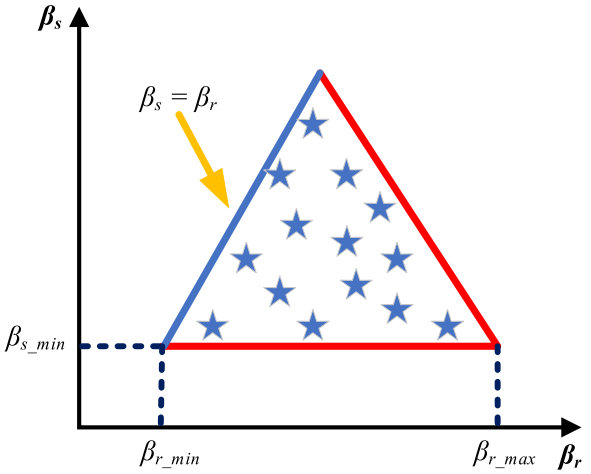

FIGURE 24. The feasible triangle of stator and rotor pole arc angles.

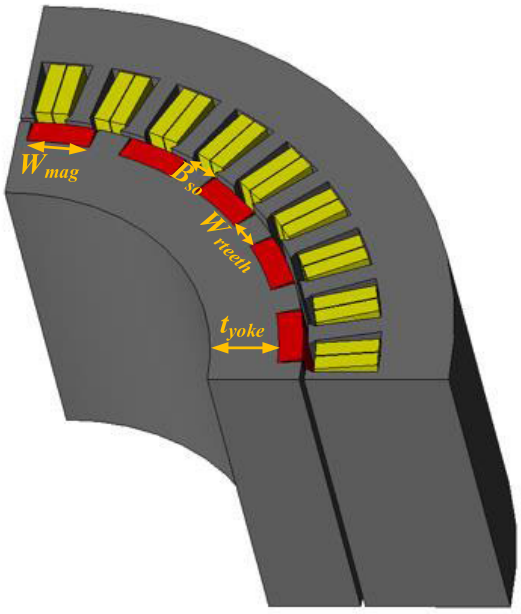

FIGURE 25. Electromagnetic model of concentrated winding PMSM.

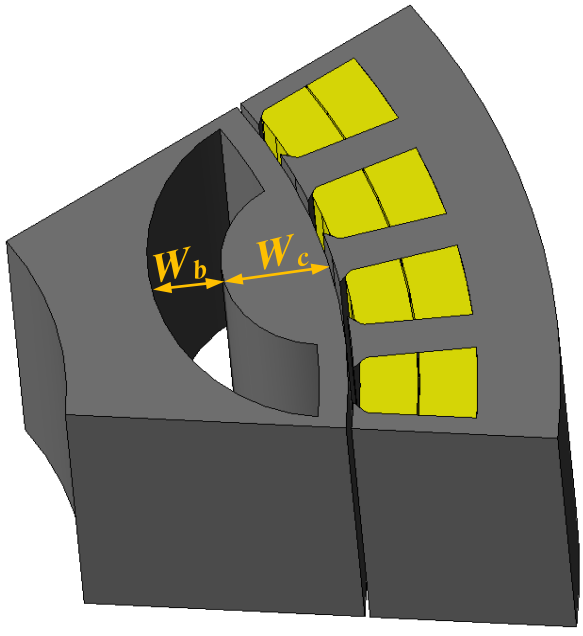

FIGURE 26. Electromagnetic model of a synchronous reluctance machine.

training. 15 data samples were used to test the GRNN. These constraints form a feasible triangle in the parameter space, as shown in Fig. 24. Table 6 compares BPNN, RBFNN, extreme learning machine (ELM), and GRNN to evaluate the effectiveness of the proposed FOA-GRNN. The results show the superiority of the FOA-GRNN model.

Besides SRMs, ML-based algorithms were also applied to design various types of electric motors. ELM and SVR approaches are suggested in [8] and [103] for the design optimization of PMSMs. The Bayesian regularization backpropagation neural network (BRNN) is adopted in the design optimization process of synchronous reluctance motors (SynRM) in [104]. ELM, SVR and BRNN proved their powerful capability to enhance the PMSM and SynRM performance. Therefore, there is a great potential to use these algorithms in design optimization of SRMs. ELM and BRNN are discussed in more detail in the coming paragraphs.

The extreme learning machine (ELM) approach is presented in [8] to design a permanent magnet synchronous linear motor (PMSLM). The structure of ELM is like FNN. However, rather than using BPNN for the learning algorithm, ELM is based on a random choice for input weights and biases. Then the output weights are determined through simple matrix computations [105]. In [8], the authors initially developed an FEA model to capture 625 data samples based on the value ranges of the selected four design geometric parameters in Table 7. The performance objectives of the proposed model were to achieve high average thrust, low total harmonic distortion, and low thrust ripple at different operating speeds. The data samples were divided into two sets. The training set utilizes 325 samples to determine the nonlinear relationship between the structural factors and output objectives. The test dataset uses 300 samples to test the model regression accuracy. Finally, a Grey Wolf Optimization Algorithm (GWOA) [8] was utilized to search for optimal performance and the best PMSLM design candidate.

A prototype was manufactured based on the optimal design candidate. The experimental results showed that the proposed method successfully achieved a good design. In addition, a comparison was conducted between the initial non-optimized model and the proposed one, and the results showed that the average thrust was increased by 12.17%. The thrust ripple and total harmonic distortion were reduced by at least 84.78% and 46.62%, respectively.

TABLE 6. Comparisons of torque ripple and performance efficiency predictions [102].

ML-based algorithms	Torque ripple Average relative error [%]	Efficiency Average relative error [%]
BPNN	4.39	1.07
RBFNN	3.61	1.01
ELM	3.28	0.78
GRNN	2.77	0.68
FOA-GRNN	0.74	0.21

TABLE 7. Variable structural design parameters [8].

Parameter to be optimized	Lower bound [mm]	Upper bound [mm]
Pole Pitch	16.0	20.0
Magnet width	13.5	15.5
Magnet height	2.0	4.0
Coil width	5.0	9.0

Another example of applying ML-based algorithms to design PMSM was introduced in [103]. SVR was employed in [103] for design optimization of a 3-kW 6-phase concentrated-winding direct-drive PMSM to meet the electric vehicle performance requirements. This work focused on using SVR as a surrogate model due to its high accuracy and effective training algorithm as compared to other models. The main idea of implementing SVR was to expand the solutions in the design space. A Pareto front method [103] was then applied to get the optimal design models with maximum torque density and minimum torque ripple.

Initially, the authors in [103] developed a hybrid analytical-FEA model. They derived analytical formulas for the average torque and the torque ripple based on inductances and flux linkages. The FEA model was invoked to estimate the 6-phase inductances and flux linkages which were used as inputs to the analytical model to calculate the average torque and torque ripple. Furthermore, multi-objective optimization was performed to get the maximum average torque and minimum torque ripple, cost, and losses. Four geometric design parameters, shown in Fig. 25, were considered to achieve these goals. The upper and lower bounds of the four variables are based on the saturation limits and basic geometrical equations of rotor yoke and stator teeth. Table 8 shows the four design variables with the related design constraints.

In [103], a parametric sweep for the four selected geometrical variables was carried out within their specified bounds to get an initial 200 design candidates using a time step FEA. Considering FEA and analytical simulations, the total computation time to obtain these 200 designs is 600 minutes. The relationship between the input geometrical variables and objectives was plotted and used to form the training and testing datasets. The training sample was used to learn the SVR and, thereby, predict further examples to boost the solution candidates in the design space [103]. The SVR optimized and generated 10,000 new design candidates in only 20 minutes. 1666 minutes were needed to obtain the same number of design candidates when using a computationally efficient FEA.

TABLE 8. Upper and lower bounds of the design parameters with their constraints [103].

Parameter to be optimized	Lower bound [mm]	Upper bound [mm]	Related constraints
Slot opening β_{so}	2.0	8.0	Stator teeth flux density $B_{teeth} < 1.7T$
Magnet pole arc length W_{mag}	11.0	17.0	Rotor yoke flux density $B_{yoke} < 0.95T$
Rotor back iron t_{yoke}	32.0	45.0	Rotor yoke flux density $B_{yoke} < 0.95T$
Rotor teeth width W_{rteeth}	12.0	15.0	Geometrical equations

The computationally efficient FEA is a fast and simplified FEA-based methodology which combines FEA with a differential evolution algorithm. It has been applied for large-scale optimization problems [106]. In addition, to receive the 10,000 design candidates using the conventional time step FEA, the time taken would be 30,000 min [103]. Thereby, the proposed method saves considerable execution time by taking only 620 minutes to create 10,200 design candidates [103]. Three optimal design candidates were recommended based on a Pareto front method [107], out of which one was chosen that achieves maximum average torque and efficiency. Then a prototype was developed for the optimal design candidate. The torque and torque ripple results from the experimental setup were recorded and compared with the results of the proposed method. The comparison showed that the discrepancy between the experiment and the proposed model in torque ripples was 4.3% at rated torque. The average torque of both models was similar [103].

In [104], BRNN was proposed to get an optimal design for a single-barrier SynRM. The regularization technique forces the ANN to converge with smaller weights and biases [108], [109]. The conventional BPNN is modified by adding a regularization step that incorporates Bayesian statistics. This overcomes the problem of overfitting and improves the generalization capability of ANN.

The chosen design parameters in [104] are the flux carrier width, W_c and barrier width, W_b, as shown in Fig. 26. The sum of these widths is constrained to avoid the possibility of intersection. The authors in [104] considered two conflicting objectives: maximizing motor average torque and minimizing its torque ripples. A 2D FEA simulation was performed to generate 48 sample points to determine the two objectives as functions of W_c and W_b. This sample data was divided randomly into 60%, 25%, and 15% for training, validation, and testing, respectively.

TABLE 9. A comparison of motor design methods.

Ref	Motor	ML-based algorithms	Design parameters	Design objectives	Dataset acquisition method / size	Results
[98]	12/8 SRM	GRNN	Pole arc angles	Maximize average torque and minimize torque ripple	2D-FEA / 35	Torque ripple reduced by 12%
[102]	12/8 SRM	FOA-GRNN	Pole arc angles and rotor yoke height	Maximize torque ripple and prediction efficiency	2D-FEA / 120	MRE of average torque is 0.74%, and prediction efficiency is 0.21%
[8]	PMSLM	GWOA-ELM	Pole Pitch, magnet width, magnet height and coil width	Maximize average thrust and minimize thrust ripple	2D-FEA / 625	Average thrust increased by 12.17%, and thrust ripple reduced by 84.78%
[103]	PMSM	SVR	Slot opening, magnet pole arc length, rotor back iron and rotor teeth width	Maximize average torque and minimize torque ripple	2D-FEA / 200	Average torque increased by 15.47%, and thrust ripple reduced by 15.2%
[104]	SynRM	GA-BRNN	Width of flux carrier and flux barrier	Maximize average torque and minimize torque ripple	2D-FEA / 48	MRE of average torque is below 0.4%, and of torque ripple is under 5.4%

Finally, A Pareto front optimization using a multi-objective GA was chosen to determine the number of rotor poles n_p [104]. Three different configurations (4, 8, and 10) for the rotor poles have been predetermined; however, only the design with an 8-pole configuration survived. The percentages of relative error between the multi-objective GA and 2D-FEA objective values were calculated. The recorded mean and standard deviation values for the average torque errors were below 0.2 and 0.1 Nm, respectively, and 5.4% and 4.0% for the torque ripple.

Table 9 summarizes the referenced papers that used ML-based algorithms in the design process of electric motors. All the mentioned papers used FEA to obtain the training dataset. The size of the dataset varies significantly. In [98] and [104], the dataset size is less than 8% of that used in [8]. The optimization objectives for all the mentioned papers are maximizing the average torque and minimizing the torque ripple. Whereas different geometrical design parameters are used due to the change of the considered motor type.

VII. POTENTIAL FUTURE RESEARCH

Based on the publications presented in this survey, SRM geometry optimization considered only the parameters directly impacting the considered objectives. This is to simplify the applied algorithm and get accurate results. Optimizing the values of more machine geometrical parameters using ML-based algorithms is still challenging and needs further work. Considering more geometrical parameters requires more training data and finite element simulations. As previously explained in [103], SVR was used in the geometry optimization of the PMSM to expand the training data space. SVR was trained based on few FEA simulations, then used to generate more data in a short time compared to the FEA [103]. This could be an effective solution to consider many SRM geometric design parameters without the need to increase the FEA simulations.

Almost all published work that applied ML-based algorithms to design the machine geometry optimally considered only two performance indicators: maximizing the average torque and minimizing the torque ripple. Therefore, adopting more indicators such as improving the machine's efficiency, reducing radial forces, or increasing torque density requires more investigation.

Since the ML-based algorithms proved their powerful capability to model the radial flux SRM, there is a strong potential for extending this application to axial flux and linear SRM topologies. In this work, there is only one mentioned article on modeling linear SRM. Moreover, according to the authors' best knowledge, there is no published work on the design optimization of the axial flux SRMs based on ML techniques. The flux in the axial flux SRMs penetrates axially from the stator to the rotor. In contrast to radial SRMs, the axial flux SRMs have relatively shorter flux paths and hence offer a higher power density [110]. Therefore, the authors expect an increase in the research and development in axial flux SRMs due to the importance and advantages of these SRMs.

Besides geometry optimization, topology optimization was applied to enhance machine performance. Several published articles used topology optimization for maximizing the SRM magnetic energy and minimizing torque ripples and vibration [111], [112], [113]. However, topology optimization algorithms suffer from a large consumption time [114]. Deep Learning, especially the convolution neural network (CNN), has gained significant attention in the topology optimization of electric machines. In [115], an CNN was adopted for the topology optimization of interior permanent magnet motor to decrease the computational effort and time. The training data of the CNN was acquired through the motor 2D images which were used in performing a preliminary topology optimization. The trained CNN was utilized to replace the FEA model. The CNN algorithm could then classify various motor models according to the model performance indices, such as

the average torque, torque ripple and motor efficiency. This technique reduced the FEA computational time by around 30% [115]. The main challenge of this algorithm is the large amount of data required to train the CNN. However, this problem was addressed in [116], [117], [118] to provide an adequate solution. To the best of authors' knowledge, the CNN algorithms were not used for SRMs. Therefore, the adoption of CNN in the topology optimization of SRMs presents an excellent opportunity for more advanced approaches.

Another potential future research can be using ML algorithms to design the complete electrical drive systems, including electrical machines, power electronic converters and control systems. Reinforcement learning has been effectively employed to drive and control electrical machines [119], [120], [121]. Reinforcement learning can be trained either from simulation or field experiments. Consequently, reinforcement learning is able to consider nonlinearities, parasitic and physical effects. Moreover, unlike model predictive control, reinforcement learning does not require an online optimization of each step, reducing the computational overhead [121]. Fellow researchers are encouraged to employ machine learning algorithms to model and drive electric motors. In other words, ML algorithms offer a good opportunity for future work as a system-level design optimization tool for electrical drive systems.

VIII. CONCLUSION

This paper presented a review of the applied machine learning algorithms in the modeling and design optimization of SRMs. Many ML-based algorithms are appropriate for modeling and design of SRMs. According to the presented and discussed studies in this paper, all applied ML-based algorithms in this field are supervised learning algorithms. The feedforward neural network and the support vector machine represent 75% of the considered articles in this paper. Most of the studies take the current and rotor position as inputs of the proposed algorithm and the torque and/or flux linkage as outputs. The sample data was either acquired using the 2D-FEA simulation or based on a locked rotor test experiment. Although the experimental method gives more accurate prediction results, it requires sophisticated sensors and tools.

The quality and size of the data samples are essential for achieving a good prediction model. Among the summarized algorithms, SVM and GRNN work well with fewer data samples. There is no general rule for splitting the sample data into training, validation, and testing sets. However, the training set commonly forms more than two-thirds of the total sample data. The training process of the neural networks is an optimization problem. Levenberg Marquardt offered the fastest and most accurate learning algorithm for backpropagation neural networks. In LSSVM, determining the kernel function and regularization parameters requires optimization algorithms as well. The RBFNN is superior in approximation ability and convergence speed. However, its significant modeling error requires a larger network scale as compared to the BPNN based on the LM learning algorithm.

The ML-based models are used as surrogates in electric motor design due to their high accuracy and effective generalization ability. The main contribution of the ML-based algorithm in this field is reducing the computational time of the design optimization process. Generally, the prediction accuracy of the ML-based algorithm and computation cost are key guidelines to assess modeling and design methods. Due to the differences between the considered methods' motor types, datasets, and output objectives, it is challenging to draw complete comparative conclusions about these methods.

REFERENCES

[1] L. Maharjan et al., "Comprehensive report on design and development of a 100-kW DSSRM," *IEEE Trans. Transport. Electrific.*, vol. 4, no. 4, pp. 835–856, Dec. 2018.
[2] C. Gan, J. Wu, Q. Sun, W. Kong, H. Li, and Y. Hu, "A review on machine topologies and control techniques for low-noise switched reluctance motors in electric vehicle applications," *IEEE Access*, vol. 6, pp. 31430–31443, 2018.
[3] B. Bilgin, J. W. Jiang, and A. Emadi, *Switched Reluctance Motor Drives: Fundamentals to Applications*. Boca Raton, FL, USA: CRC Press, 2019.
[4] P. C. Kjaer, J. J. Gribble, and T. J. E. Miller, "Dynamic testing of switched reluctance motors for high-bandwidth actuator applications," *IEEE/ASME Trans. Mechatronics*, vol. 2, no. 2, pp. 123–135, Jun. 1997.
[5] Z. Rahman, M. Ehsani, and K. L. Butler, "An investigation of electric motor drive characteristics for EV and HEV propulsion systems," in *Proc. Future Transp. Techno. Conf. Expo.*, Costa Mesa, CA, USA, Aug. 2000, pp. 1–10.
[6] B. Bilgin, J. Liang, M. V. Terzic, J. Dong, R. Rodriguez, E. Trickett, and A. Emadi, "Modeling and analysis of electric motors: State-of-the-art review," *IEEE Trans. Transport. Electrific.*, vol. 5, no. 3, pp. 602–617, Sep. 2019.
[7] Y. Duan and D. M. Ionel, "A review of recent developments in electrical machine design optimization methods with a permanent-magnet synchronous motor benchmark study," *IEEE Trans. Ind. Appl.*, vol. 49, no. 3, pp. 1268–1275, May/Jun. 2013.
[8] J. Song, F. Dong, J. Zhao, H. Wang, Z. He, and L. Wang, "An efficient multiobjective design optimization method for a PMSLM based on an extreme learning machine," *IEEE Trans. Ind. Electron.*, vol. 66, no. 2, pp. 1001–1011, Feb. 2019.
[9] S. R. Mousavi-Aghdam, M. R. Feyzi, N. Bianchi, and M. Morandin, "Design and analysis of a novel high-torque stator-segmented SRM," *IEEE Trans. Ind. Electron.*, vol. 63, no. 3, pp. 1458–1466, Mar. 2016.
[10] M. J. Kamper, S. W. Rasmeni, and R. J. Wang, "Finite-element time-step simulation of the switched reluctance machine drive under single pulse mode operation," *IEEE Trans. Magn.*, vol. 43, no. 7, pp. 3202–3208, Jul. 2007.
[11] E. Afjei, A. Siadatan, and H. Torkaman, "Magnetic modeling, prototyping, and comparative study of a quintuple-set switched reluctance motor," *IEEE Trans. Magn.*, vol. 51, no. 8, pp. 1–7, Aug. 2015.
[12] G. Lei, C. Liu, J. Zhu, and Y. Guo, "Techniques for multilevel design optimization of permanent magnet motors," *IEEE Trans. Energy Convers.*, vol. 30, no. 4, pp. 1574–1584, Dec. 2015.
[13] O. Ustun, "Measurement and real-time modeling of inductance and flux linkage in switched reluctance motors," *IEEE Trans. Magn.*, vol. 45, no. 12, pp. 5376–5382, Dec. 2009.
[14] A. Khalil and I. Husain, "A Fourier series generalized geometry-based analytical model of switched reluctance machines," *IEEE Trans. Ind. Appl.*, vol. 43, no. 3, pp. 673–684, May/Jun. 2007.
[15] V. P. Vujicic, "Modeling of a switched reluctance machine based on the invertible torque function," *IEEE Trans. Magn.*, vol. 44, no. 9, pp. 2186–2194, Sep. 2008.
[16] M. Yilmaz and P. T. Krein, "Capabilities of finite element analysis and magnetic equivalent circuits for electrical machine analysis and design," in *Proc. IEEE Power Electron. Spec. Conf.*, Rhodes, Greece, Jun. 2008, pp. 4027–4033.
[17] Y. Zhang, K. T. Chau, J. Z. Jiang, D. Zhang, and C. Liu, "A finite element–analytical method for electromagnetic field analysis of electric machines with free rotation," *IEEE Trans. Magn.*, vol. 42, no. 10, pp. 3392–3394, Oct. 2006.

[18] M. E. Abdollahi, N. Vaks, and B. Bilgin, "A multi-objective optimization framework for the design of a high power-density switched reluctance motor," in *Proc. IEEE Transp. Electrific. Conf. Expo (ITEC)*, Anaheim, CA, USA, Jun. 2022, pp. 67–73.

[19] M. Tahkola, J. Keranen, D. Sedov, M. F. Far, and J. Kortelainen, "Surrogate modeling of electrical machine torque using artificial neural networks," *IEEE Access*, vol. 8, pp. 220027–220045, 2020.

[20] J. W. Jiang, B. Bilgin, and A. Emadi, "Three-phase 24/16 switched reluctance machine for a hybrid electric powertrain," *IEEE Trans. Transport. Electrific.*, vol. 3, no. 1, pp. 76–85, Mar. 2017.

[21] O. Zayed, M. Omar, M. Bakr, M. Narimani, A. Emadi, and B. Bilgin, "Switched reluctance motor design for an EV propulsion application," in *Proc. 47th Annu. Conf. IEEE Ind. Electron. Soc.*, Toronto, ON, Canada,Oct. 2021, pp. 1–6.

[22] E. Sayed, M. Abdalmagid, G. Pietrini, N.-M. Sa'adeh, A. D. Callegaro, C. Goldstein, and A. Emadi, "Review of electric machines in more-/hybrid-/turbo-electric aircraft," *IEEE Trans. Transport. Electrific.*, vol. 7, no. 4, pp. 2976–3005, Dec. 2021.

[23] J. K. Nøland, M. Leandro, and J. A. Suul, "High-power machines and starter-generator topologies for more electric aircraft: A technology outlook," *IEEE Access*, vol. 8, pp. 130104–130123, 2020.

[24] J. D. Widmer, R. Martin, and B. C. Mecrow, "Optimization of an 80-kW segmental rotor switched reluctance machine for automotive traction," *IEEE Trans. Ind. Appl.*, vol. 51, no. 4, pp. 2990–2999, Jul./Aug. 2015.

[25] B. Bilgin, A. Emadi, and M. Krishnamurthy, "Design considerations for switched reluctance machines with a higher number of rotor poles," *IEEE Trans. Ind. Electron.*, vol. 59, no. 10, pp. 3745–3756, Oct. 2012.

[26] J. B. Bartolo, M. Degano, J. Espina, and C. Gerada, "Design and initial testing of a high-speed 45-kW switched reluctance drive for aerospace application," *IEEE Trans. Ind. Electron.*, vol. 64, no. 2, pp. 988–997, Feb. 2017.

[27] B. Bilgin, B. Howey, A. D. Callegaro, J. Liang, M. Kordic, J. Taylor, and A. Emadi, "Making the case for switched reluctance motors for propulsion applications," *IEEE Trans. Veh. Technol.*, vol. 69, no. 7, pp. 7172–7186, Jul. 2020.

[28] G. Watthewaduge, E. Sayed, A. Emadi, and B. Bilgin, "Electromagnetic modeling techniques for switched reluctance machines: State-of-the-art review," *IEEE Open J. Ind. Electron. Soc.*, vol. 1, pp. 218–234, 2020.

[29] S. Li, S. Zhang, T. G. Habetler, and R. G. Harley, "Modeling, design optimization, and applications of switched reluctance machines—A review," *IEEE Trans. Ind. Appl.*, vol. 55, no. 3, pp. 2660–2681, Jun. 2019.

[30] K. Hameyer and R. Belmans, *Numerical Modelling and Design of Electrical Machines and Devices*, vol. 1. Boston, MA, USA: WIT Press, 1999.

[31] N. Bianchi, *Electrical Machine Analysis Using Finite Elements*. Boca Raton, FL, USA: CRC Press, 2005.

[32] H. P. Chi, R. L. Lin, and J. F. Chen, "Simplified flux-linkage model for switched-reluctance motors," *IEE Proc. Electr. Power Appl.*, vol. 152, no. 3, pp. 577–583, Mar. 2005.

[33] T. C. O'Connell and P. T. Krein, "A time-harmonic three-dimensional vector boundary element model for electromechanical devices," *IEEE Trans. Energy Convers.*, vol. 25, no. 3, pp. 606–618, Sep. 2010.

[34] D. M. Araujo, J.-L. Coulomb, O. Chadebec, and L. Rondot, "A hybrid boundary element method-reluctance network method for open boundary 3-D nonlinear problems," *IEEE Trans. Magn.*, vol. 50, no. 2, pp. 77–80, Feb. 2014.

[35] D. Wang, D. Zhang, X. Du, and X. Wang, "Unitized design methodology of linear switched reluctance motor with segmental secondary for long rail propulsion application," *IEEE Trans. Ind. Electron.*, vol. 65, no. 12, pp. 9884–9894, Dec. 2018.

[36] W. Uddin, T. Husain, Y. Sozer, and I. Husain, "Design methodology of a switched reluctance machine for off-road vehicle applications," *IEEE Trans. Ind. Appl.*, vol. 52, no. 3, pp. 2138–2147, May 2016.

[37] Z. Zhang and Y. Li, "Numerical and analytical modeling of switched reluctance machines," *J. Comput.*, vol. 7, no. 12, pp. 3036–3043, Dec. 2012.

[38] Y. Yang and A. Emadi, "Coupled switched reluctance machine modeling and simulations," in *Proc. IEEE Conf. Expo Transp. Electrific. Asia–Pacific (ITEC Asia-Pacific)*, Beijing, China, Aug. 2014, pp. 1–6.

[39] X.-D. Xue, K. W. E. Cheng, and S. L. Ho, "Simulation of switched reluctance motor drives using two-dimensional bicubic spline," *IEEE Trans. Energy Convers.*, vol. 17, no. 4, pp. 471–477, Dec. 2002.

[40] J. M. Stephenson and J. Čorda, "Computation of torque and current in doubly salient reluctance motors from nonlinear magnetisation data," *Proc. Inst. Elect. Eng.*, vol. 126, no. 5, pp. 393–396, May 1979.

[41] W. Lu, A. Keyhani, and A. Fardoun, "Neural network-based modeling and parameter identification of switched reluctance motors," *IEEE Trans. Energy Convers.*, vol. 18, no. 2, pp. 284–290, Jun. 2003.

[42] M. Mohri, A. Rostamizadeh, and A. Talwalkar, *Foundations of Machine Learning*. 2nd ed. Cambridge, MA, USA: MIT Press, 2018.

[43] C. M. Bishop, *Pattern Recognition and Machine Learning*. New York, NY, USA: Springer, 2006.

[44] R. S. Sutton and A. G. Barto, *Reinforcement Learning: An Introduction*. Boston, MA, USA: MIT Press, 1998.

[45] I. Goodfellow, Y. Bengio, and A. Courville, *Deep Learning*. Cambridge, MA, USA: MIT Press, 2016.

[46] M. Bakr, *Nonlinear Optimization in Electrical Engineering With Applications in MATLAB*. London, U.K.: Institution of Engineering and Technology, 2013.

[47] C. Harpham, C. W. Dawson, and M. R. Brown, "A review of genetic algorithms applied to training radial basis function networks," *Neural Comput. Appl.*, vol. 13, pp. 193–201, Apr. 2004.

[48] Y. Cai, Y. Wang, H. Xu, S. Sun, C. Wang, and L. Sun, "Research on rotor position model for switched reluctance motor using neural network," *IEEE/ASME Trans. Mechatronics*, vol. 23, no. 6, pp. 2762–2773, Dec. 2018.

[49] Y. Cai and C. Gao, "Nonlinear modeling of switched reluctance motor based on BP neural network," in *Proc. 3rd Int. Conf. Natural Comput. (ICNC)*, Haikou, China, 2007, pp. 232–236.

[50] Y. Cai and C. Gao, "Torque ripple minimization in switched reluctance motor based on BP neural network," in *Proc. 2nd IEEE Conf. Ind. Electron. Appl.*, Harbin, China, May 2007, pp. 1198–1202.

[51] T. Lachman, T. R. Mohamad, and C. H. Fong, "Nonlinear modelling of switched reluctance motors using artificial intelligence techniques," *IEE Proc. Electr. Power App.*, vol. 151, no. 1, pp. 6–53, Jan. 2004.

[52] L. A. Zadeh, "Fuzzy algorithms," *Inf. Control*, vol. 12, no. 2, pp. 94–102, Feb. 1968.

[53] Z. Zhihui and L. Yuren, "Modeling and simulation of switched reluctance machine based aircraft electric brake system by BP neural network," in *Proc. 9th IEEE Conf. Ind. Electron. Appl.*, Hangzhou, China, Jun. 2014, pp. 338–341.

[54] E. Mese and D. A. Torrey, "An approach for sensorless position estimation for switched reluctance motors using artifical neural networks," *IEEE Trans. Power Electron.*, vol. 17, no. 1, pp. 66–75, Jan. 2002.

[55] D. A. Torrey and J. H. Lang, "Modelling a nonlinear variable-reluctance motor drive," in *Proc. IEE B, Electr. Power*, vol. 137, pp. 314–326, Sep. 1990.

[56] C. Elmas, S. Sagiroglu, I. Colak, and G. Bal, "Modelling of a nonlinear switched reluctance drive based on artificial neural networks," in *Proc. 5th Int. Conf. Power Electron. Variable-Speed Drives*, London, U.K., Oct. 1994, pp. 7–12.

[57] W. Xilian, Z. Yihuang, L. Huijuan, and H. Hui, "Nonlinear modeling of switched reluctance motor based on combination of neural network and genetic algorithm," in *Proc. Int. Conf. Electr. Mach. Syst.*, Nanjing, China, Sep. 2005, pp. 572–574.

[58] S. Qi and H. Kong, "A modeling method of SRM based on RBF neural networks," in *Proc. Int. Conf. Electron., Commun. Control (ICECC)*, Ningbo, China, Sep. 2011, pp. 44–47.

[59] S. Zhou, "Modeling of switched reluctance motor based on combined clustering RBF network," in *Proc. 20th Int. Conf. Electr. Mach. Syst. (ICEMS)*, Sydney, NSW, Australia, Aug. 2017, pp. 1–5.

[60] J. Cai, Z. Q. Deng, R. Y. Qi, Z. Y. Liu, and Y. H. Cai, "A novel BVC-RBF neural network based system simulation model for switched reluctance motor," *IEEE Trans. Magn.*, vol. 47, no. 4, pp. 830–838, Apr. 2011.

[61] X. Zhang, F. Wang, and X. Shao, "Flux linkage characteristics on-line modeling of switched reluctance motor based on boundary constraints RBF," in *Proc. 11th World Congr. Intell. Control Autom.*, Shenyang, China, Jun. 2014, pp. 5942–5946.

[62] F. Yang, W. Li, C. Li, and Q. Miao, "State-of-charge estimation of lithium-ion batteries based on gated recurrent neural network," *Energy*, vol. 175, pp. 66–75, May 2019.

[63] I. J. Myung, "Tutorial on maximum likelihood estimation," *J. Math. Psychol.*, vol. 47, no. 1, pp. 90–100, Feb. 2003.

[64] F. Daldaban, N. Ustkoyuncu, and K. Guney, "Phase inductance estimation for switched reluctance motor using adaptive neuro-fuzzy inference system," *Energy Convers. Manage.*, vol. 47, no. 5, pp. 485–493, Mar. 2006.

[65] J. Wu, X. Sun, and J. Zhu, "Accurate torque modeling with PSO-based recursive robust LSSVR for a segmented-rotor switched reluctance motor," *CES Trans. Electr. Mach. Syst.*, vol. 4, no. 2, pp. 96–104, Jun. 2020.
[66] W. Ding and D. Liang, "Modeling of a 6/4 switched reluctance motor using adaptive neural fuzzy inference system," *IEEE Trans. Magn.*, vol. 44, no. 7, pp. 1796–1804, Jul. 2008.
[67] D. Liang and W. Ding, "Modelling and predicting of a switched reluctance motor drive using radial basis function network-based adaptive fuzzy system," *IET Electr. Power App.*, vol. 3, pp. 218–230, May 2009.
[68] C. Cortes and V. Vapnik, "Support-vector networks," *Mach. Learn.*, vol. 20, no. 3, pp. 273–297, 1995.
[69] M. Li, R. Guo, K. Zhang, Z. Lin, F. Yang, S. Xu, X. Chen, A. Massa, and A. Abubakar, "Machine learning in electromagnetics with applications to biomedical imaging: A review," *IEEE Antennas Propag. Mag.*, vol. 63, no. 3, pp. 39–51, Jun. 2021.
[70] A. Soualhi, K. Medjaher, and N. Zerhouni, "Bearing health monitoring based on Hilbert–Huang transform, support vector machine, and regression," *IEEE Trans. Instrum. Meas.*, vol. 64, no. 1, pp. 52–62, Jan. 2015.
[71] M. Kang, J. Kim, J.-M. Kim, A. C. C. Tan, E. Y. Kim, and B.-K. Choi, "Reliable fault diagnosis for low-speed bearings using individually trained support vector machines with kernel discriminative feature analysis," *IEEE Trans. Power Electron.*, vol. 30, no. 5, pp. 2786–2797, May 2015.
[72] R. Solera-Urena, A. I. Garcia-Moral, C. Pelaez-Moreno, M. Martinez-Ramon, and F. Diaz-de-Maria, "Real-time robust automatic speech recognition using compact support vector machines," *IEEE Trans. Audio, Speech, Language Process.*, vol. 20, no. 4, pp. 1347–1361, May 2012.
[73] Y.-H. Liu, H.-P. Huang, and C.-H. Weng, "Recognition of electromyographic signals using cascaded kernel learning machine," *IEEE/ASME Trans. Mechatronics*, vol. 12, no. 3, pp. 253–264, Jun. 2007.
[74] Q. Ye, Z. Han, J. Jiao, and J. Liu, "Human detection in images via piecewise linear support vector machines," *IEEE Trans. Image Process.*, vol. 22, no. 2, pp. 778–789, Feb. 2013.
[75] S. Song, L. Ge, and M. Zhang, "Data-reconstruction-based modeling of SRM with few flux-linkage samples from torque-balanced measurement," *IEEE Trans. Energy Convers.*, vol. 31, no. 2, pp. 424–435, Jun. 2016.
[76] J. A. K. Suykens and J. Vandewalle, "Least squares support vector machine classifiers," *Neural Process. Lett.*, vol. 9, no. 3, pp. 293–300, Jun. 1999.
[77] J. Valyon and G. Horváth, "Extended least squares LS-SVM," *Int. J. Comput. Intell.*, vol. 3, pp. 234–242, Jul. 2005.
[78] C. Xie, C. Shao, and D. Zhao, "Parameters optimization of least squares support vector machines and its application," *J. Comput.*, vol. 6, no. 9, pp. 1935–1941, Aug. 2011.
[79] L. Si, H. Liu, and Z. Liu, "Modeling of switched reluctance motors based on LS-SVM," *Proc. Chin. Soc. Electr. Eng.*, vol. 27, no. 6, pp. 26–30, 2007.
[80] W. Shang, S. Zhao, and Y. Shen, "Application of LSSVM with AGA optimizing parameters to nonlinear modeling of SRM," in *Proc. 3rd IEEE Conf. Ind. Electron. Appl.*, Singapore, Jun. 2008, pp. 775–780.
[81] H. Likun, Y. Qingxin, and A. Jinlong, "Modeling of SRM based on XS-LSSVR optimized by GDS," *IEEE Trans. Appl. Supercond.*, vol. 20, no. 3, pp. 1102–1105, Jun. 2010.
[82] Q. Xiang, Y. Sun, and X. Ji, "Modeling inductance for bearingless switched reluctance motor based on PSO-LSSVM," in *Proc. Chin. Control Decis. Conf. (CCDC)*, Mianyang, China, May 2011, pp. 800–803.
[83] R. Zhong, Y.-P. Cao, W. Hua, Y.-Z. Xu, and S. Xu, "An improved model of switched reluctance motors based on least square support vector machine," in *Proc. IEEE Int. Symp. Ind. Electron.*, Taiwan, May 2013, pp. 1–6.
[84] R. Mall and J. A. K. Suykens, "Very sparse LSSVM reductions for large-scale data," *IEEE Trans. Neural Netw. Learn. Syst.*, vol. 26, no. 5, pp. 1086–1097, May 2015.
[85] G. Si, J. Shi, Z. Guo, L. Jia, and Y. Zhang, "Reconstruct the support vectors to improve LSSVM sparseness for mill load prediction," *Math. Problems Eng.*, vol. 2017, p. 12, Jul. 2017.
[86] J. A. K. Suykens, L. Lukas, and J. Vandewalle, "Sparse approximation using least squares support vector machines," in *Proc. IEEE Int. Symp. Circuits Syst. (ISCAS)*, vol. 2, Geneva, Switzerland, 2000, pp. 757–760.
[87] S. D. Huang, G. Z. Cao, Z. Y. He, J. F. Pan, J. A. Duan, and Q. Q. Qian, "Nonlinear modeling of the inverse force function for the planar switched reluctance motor using sparse least squares support vector machines," *IEEE Trans. Ind. Informat.*, vol. 11, no. 3, pp. 591–600, Jun. 2015.
[88] J. E. Stephen, S. S. Kumar, and J. Jayakumar, "Nonlinear modeling of a switched reluctance motor using LSSVM—ABC," *Acta Polytechnica Hungarica*, vol. 11, no. 6, pp. 1–16, 2014.
[89] D. Karaboga, B. Gorkemli, C. Ozturk, and N. Karaboga, "A comprehensive survey: Artificial bee colony (ABC) algorithm and applications," *Artif. Intell. Rev.*, vol. 42, no. 1, pp. 21–57, 2014.
[90] J. E. Stephen, S. S. Kumar, and J. Jayakumar, "Torque modeling of switched reluctance motor using LSSVM-DE," *Neurocomputing*, vol. 211, pp. 117–128, Oct. 2016.
[91] X. Sun, J. Wu, G. Lei, Y. Cai, X. Chen, and Y. Guo, "Torque modeling of a segmented-rotor SRM using maximum-correntropy-criterion-based LSSVR for torque calculation of EVs," *IEEE J. Emerg. Sel. Topics Power Electron.*, vol. 9, no. 3, pp. 2674–2684, Jun. 2021.
[92] S. Mirjalili, S. M. Mirjalili, and A. Lewis, "Grey wolf optimizer," *Adv. Eng. Softw.*, vol. 69, pp. 46–61, Mar. 2014.
[93] B. Chen, X. Wang, Y. Li, and J. C. Principe, "Maximum correntropy criterion with variable center," *IEEE Signal Process. Lett.*, vol. 26, no. 5, pp. 1212–1216, Aug. 2019.
[94] C. Vidal, P. Malysz, P. Kollmeyer, and A. Emadi, "Machine learning applied to electrified vehicle battery state of charge and state of health estimation: State-of-the-art," *IEEE Access*, vol. 8, pp. 52796–52814, 2020.
[95] J. W. Bandler, Q. S. Cheng, S. A. Dakroury, A. S. Mohamed, M. H. Bakr, K. Madsen, and J. Sondergaard, "Space mapping: The state of the art," *IEEE Trans. Microw. Theory Techn.*, vol. 52, no. 1, pp. 337–361, Jan. 2004.
[96] J. Gong, H. Zhang, B. Zhao, D. Fu, and F. Gillon, "Proposal of a bi-objective Kriging adapted output space mapping technique for electromagnetic design optimization," *IEEE Trans. Magn.*, vol. 55, no. 6, pp. 1–5, Jun. 2019.
[97] M. Li, F. Gabriel, M. Alkadri, and D. A. Lowther, "Kriging-assisted multi-objective design of permanent magnet motor for position sensorless control," *IEEE Trans. Magn.*, vol. 52, no. 3, pp. 1–4, Mar. 2016.
[98] H. Sahraoui, H. Zeroug, and H. A. Toliyat, "Switched reluctance motor design using neural-network method with static finite-element simulation," *IEEE Trans. Magn.*, vol. 43, no. 12, pp. 4089–4095, Dec. 2007.
[99] D. F. Specht, "A general regression neural network," *IEEE Trans. Neural Netw.*, vol. 2, no. 6, pp. 568–576, Nov. 1991.
[100] B.-G. Hyun and K. Nam, "Faults diagnoses of rotating machines by using neural nets: GRNN and BPN," in *Proc. 21st Annu. Conf. IEEE Ind. Electron. (IECON)*, Orlando, FL, USA, Nov. 1995, pp. 1456–1461.
[101] E. Sayed, P. Azer, M. Kordic, J. Reimers, B. Bilgin, M. H. Bakr, and A. Emadi, "Design of a switched reluctance motor for a pump Jack application," in *Proc. IEEE Electr. Power Energy Conf. (EPEC)*, Toronto, ON, Canada, Oct. 2018, pp. 1–6.
[102] Z. Zhang, S. Rao, and X. Zhang, "Performance prediction of switched reluctance motor using improved generalized regression neural networks for design optimization," *CES Trans. Electr. Mach. Syst.*, vol. 2, no. 4, pp. 371–376, Dec. 2018.
[103] H. Dhulipati, E. Ghosh, S. Mukundan, P. Korta, J. Tjong, and N. C. Kar, "Advanced design optimization technique for torque profile improvement in six-phase PMSM using supervised machine learning for direct-drive EV," *IEEE Trans. Energy Convers.*, vol. 34, no. 4, pp. 2041–2051, Dec. 2019.
[104] M. H. Mohammadi, T. Rahman, R. Silva, M. Li, and D. A. Lowther, "A computationally efficient algorithm for rotor design optimization of synchronous reluctance machines," *IEEE Trans. Magn.*, vol. 52, no. 3, pp. 1–4, Mar. 2016.
[105] G.-B. Huang, Q.-Y. Zhu, and C.-K. Siew, "Extreme learning machine: Theory and applications," *Neurocomputing*, vol. 70, nos. 1–3, pp. 489–501, 2006.
[106] P. Zhang, G. Y. Sizov, M. Li, D. M. Ionel, N. A. O. Demerdash, S. J. Stretz, and A. W. Yeadon, "Multi-objective tradeoffs in the design optimization of a brushless permanent-magnet machine with fractional-slot concentrated windings," *IEEE Trans. Ind. Appl.*, vol. 50, no. 5, pp. 3285–3294, Sep./Oct. 2014.
[107] I. Y. Kim and O. L. D. Weck, "Adaptive weighted-sum method for bi-objective optimization: Pareto front generation," *Struct. Multidisciplinary Optim.*, vol. 29, no. 2, pp. 149–158, Feb. 2005.

[108] N. B. D. Choudhury and S. K. Goswami, "Transmission loss allocation using Bayesian regularization backpropagation ANN," in *Proc. Annu. IEEE India Conf. (INDICON)*, Kolkata, India, Dec. 2010, pp. 1–4.
[109] F. Burden and D. Winkler, "Bayesian regularization of neural networks," in *Artificial Neural Networks*, vol. 458. Totowa, NJ, USA: Humana Press, 2008, pp. 23–42.
[110] B. Wang, D.-H. Lee, C.-W. Lee, and J.-W. Ahn, "Characteristics analysis of a novel segmental rotor axial field switched reluctance motor with single teeth winding," *J. Power Electron.*, vol. 14, no. 5, pp. 852–858, Sep. 2014.
[111] J.-K. Byun and S.-Y. Hahn, "Topology optimization of switched reluctance motor using mutual energy method," *Int. J. Appl. Electromagn. Mech.*, vol. 13, nos. 1–4, pp. 421–426, Dec. 2002.
[112] J. Lee, J. H. Seo, and N. Kikuchi, "Topology optimization of switched reluctance motors for the desired torque profile," *Struct. Multidisciplinary Optim.*, vol. 42, no. 5, pp. 783–796, 2010.
[113] J. Yoo, "Reduction of vibration caused by magnetic force in a switched reluctance motor by topology optimization," *J. Appl. Mech.*, vol. 69, no. 3, pp. 380–387, May 2002.
[114] M. Abdalmagid, E. Sayed, M. H. Bakr, and A. Emadi, "Geometry and topology optimization of switched reluctance machines: A review," *IEEE Access*, vol. 10, pp. 5141–5170, 2022.
[115] H. Sasaki and H. Igarashi, "Topology optimization accelerated by deep learning," *IEEE Trans. Magn.*, vol. 55, no. 6, pp. 1–5, Jun. 2019.
[116] J. Asanuma, S. Doi, and H. Igarashi, "Transfer learning through deep learning: Application to topology optimization of electric motor," *IEEE Trans. Magn.*, vol. 56, no. 3, pp. 1–4, Mar. 2020.
[117] D. Zhong, Y. Yang, and X. Du, "Palmprint recognition using Siamese network," in *Proc. Chin. Conf. Biometric Recognit.*, Ürümqi, China, 2018, pp. 48–55.
[118] S. Doi, H. Sasaki, and H. Igarashi, "Multi-objective topology optimization of rotating machines using deep learning," *IEEE Trans. Magn.*, vol. 55, no. 6, pp. 1–5, Jun. 2019.
[119] Y. Li, G. Lei, G. Bramerdorfer, S. Peng, X. Sun, and J. Zhu, "Machine learning for design optimization of electromagnetic devices: Recent developments and future directions," *Appl. Sci.*, vol. 11, no. 4, p. 1627, Feb. 2021.
[120] M. Schenke, W. Kirchgässner, and O. Wallscheid, "Controller design for electrical drives by deep reinforcement learning: A proof of concept," *IEEE Trans. Ind. Informat.*, vol. 16, no. 7, pp. 4650–4658, Jul. 2020.
[121] A. Traue, G. Book, W. Kirchgässner, and O. Wallscheid, "Toward a reinforcement learning environment toolbox for intelligent electric motor control," *IEEE Trans. Neural Netw. Learn. Syst.*, vol. 33, no. 3, pp. 919–928, Mar. 2022.

MOHAMED OMAR (Graduate Student Member, IEEE) received the B.Sc. degree (Hons.) in electrical engineering from the Shoubra Faculty of Engineering, Benha University, Cairo, Egypt, in 2011, and the M.Sc. degree in electrical engineering from Cairo University, Egypt, in 2017. He is currently pursuing the Ph.D. degree in electrical engineering with the McMaster Automotive Resource Centre (MARC), McMaster University, ON, Canada. After his bachelor's degree, he worked as an Assistant Researcher at the Electronics Research Institute, Cairo. He is involved in an industrial project, where he performs the design and testing of Solid-State Power Converters (SSPC) for an aerospace application. His main research interest includes design and modeling of switched reluctance motors using machine learning.

EHAB SAYED (Member, IEEE) received the B.Sc. degree (Hons.) in electrical engineering and the M.Sc. degree in electrical engineering, electrical machines and drive systems specialization from the Shoubra Faculty of Engineering, Benha University, Egypt, in 2010 and 2016, respectively, and the Ph.D. degree in electrical engineering from McMaster University, ON, Canada, in 2019. He worked as a Teaching Assistant and a Research Assistant at Benha University, from 2012 to 2016. While pursuing the degree, he was involved in many industrial projects, where he designed various types of electric machines for different applications. He worked as a Postdoctoral Fellow at the McMaster Automotive/Aerospace Resource Centre, where his research interest was the design of electric machines for automotive/aerospace applications. He is currently an Assistant Professor at the Shoubra Facuty of Engineering, Benha University, where his focus is the design and drive of electric machines.

MOHAMED ABDALMAGID (Graduate Student Member, IEEE) received the B.Sc. degree (Hons.) in electrical engineering from the Shoubra Faculty of Engineering, Benha University, Cairo, Egypt, in 2011, and the M.Sc. degree in electrical engineering from the Faculty of Engineering, Cairo University, Giza, Egypt, in 2017. He is currently pursuing the Ph.D. degree in electrical engineering with the McMaster Automotive/Aerospace Resource Centre, McMaster University, Hamilton, ON, Canada.

He was a Research Assistant at the Electronics Research Institute, Cairo, from 2013 to 2018. He is involved in many industrial projects, where he designs and tests various configurations of axial flux permanent magnet motor for aerospace propulsion application. His research interests include axial flux permanent magnet (PM) motor design, switched reluctance motor (SRM) design, and optimization of SRM design for automotive/aerospace applications.

BERKER BILGIN (Senior Member, IEEE) received the Ph.D. degree in electrical engineering from the Illinois Institute of Technology, Chicago, IL, USA, in 2011, and the M.B.A. degree from the DeGroote School of Business, McMaster University, Hamilton, ON, Canada, in 2018.

He is an Assistant Professor with the Department of Electrical and Computer Engineering (ECE), McMaster University. He is also the Co-Founder and the Vice President of engineering at Enedym Inc., Hamilton, which is a spin-off company of McMaster University. Enedym specializes in electric machines, electric motor drives (EMDs), advanced controls and software, and virtual engineering. He has authored and coauthored 127 journals and conference papers and three book chapters. He is the Lead Editor and the Author of the textbook titled *SRM Drives: Fundamentals to Applications*. He is the Principal Inventor/the Co-Inventor of ten patents and pending patent applications. His current research interests include electric machines, switched reluctance motor (SRM) drives, acoustic noise and vibration analysis and reduction, power electronics, and EMDs.

Dr. Bilgin was the Elected General Chair of the 2016 IEEE Transportation Electrification Conference and Expo (ITEC). He serves as an Associate Editor for the IEEE TRANSACTIONS ON TRANSPORTATION ELECTRIFICATION.

MOHAMED H. BAKR (Senior Member, IEEE) received the B.Sc. degree (Hons.) in electronics and communications engineering and the master's degree in engineering mathematics from Cairo University, Egypt, in 1992 and June 1996, respectively, and the Ph.D. degree from the Department of Electrical and Computer Engineering, McMaster University, Hamilton, ON, Canada, in September 2000. In 1997, he was a Student Intern with Optimization Systems Associates (OSA) Inc. From 1998 to 2000, he worked as a Research Assistant with the Simulation Optimization Systems (SOS) Research Laboratory, McMaster University. In November 2000, he joined the Computational Electromagnetics Research Laboratory (CERL), University of Victoria, Victoria, Canada, as an NSERC Postdoctoral Fellow. He is currently working as a Professor with the Department of Electrical and Computer Engineering, McMaster University. He is the author/the coauthor of over 290 journals and conference papers, two books on the optimization and CAD of high frequency structures, three book chapters on optimization, electromagnetic modeling, and artificial intelligence and two patents. His research interests include optimization methods, computational electromagnetics, computer-aided design, modeling of power circuits and motors, microwave circuits, THz, and photonic devices, nanotechnology, artificial intelligence and its applications, smart analysis of high frequency structures, and efficient optimization using time/frequency domain methods. He received the Premier's Research Excellence Award (PREA) from the province of Ontario, Canada, in 2003. He also received the NSERC Discovery Accelerator Supplement (DAS) Award in 2011. In 2014, he was a Co-recipient of the Chrysler's Innovation Award for the project on novel designs of hybrid cars. In 2015, he was listed on the Dean's Teaching Honour Roll several times in recognition of his success in utilizing flipped classrooms to teaching engineering courses. He was awarded a Leadership in Teaching and Learning (LTL) Fellowship from the McPherson Institute, McMaster University, in April 2018. In 2020, he was a recipient of the Faculty Appreciation Award by the McMaster Engineering Society (MES). In April 2021, he was awarded the President's Award for Outstanding Contributions for Teaching and Learning from McMaster University. In July 2021, he was awarded a Distinguished Engineering Educator Honorific from the Faculty of Engineering, McMaster University. He was also included in Stanford's list of the top 2% most cited scientists for the years 2020 and 2022. He was selected as the Chair of the Department of Electrical and Computer Engineering, McMaster University, for five years in July 2022.

ALI EMADI (Fellow, IEEE) received the B.S. and M.S. degrees (Hons.) in electrical engineering from the Sharif University of Technology, Tehran, Iran, in 1995 and 1997, respectively, and the Ph.D. degree in electrical engineering from Texas A&M University, College Station, TX, USA, in 2000. He is currently the Canada Excellence Research Chair Laureate at McMaster University, Hamilton, ON, Canada. He is also the holder of the NSERC/FCA Industrial Research Chair in electrified powertrains and the Tier I Canada Research Chair in transportation electrification and smart mobility. Before joining McMaster University, he was the Harris Perlstein Endowed Chair Professor of engineering and the Director of the Electric Power and Power Electronics Center; and Grainger Laboratories, Illinois Institute of Technology, Chicago, where he established research and teaching facilities and courses in power electronics, motor drives, and vehicular power systems. He was the Founder, the Chairperson, and the President of Hybrid Electric Vehicle Technologies, Inc. (HEVT)—a university spin-off company of Illinois Tech. He is the President and the Chief Executive Officer of Enedym Inc., and Menlolab Inc.—two McMaster University spin-off companies. He is the principal author/the coauthor of over 500 journals and conference papers and several books, including *Vehicular Electric Power Systems* (2003), *Energy Efficient Electric Motors* (2004), *Uninterruptible Power Supplies and Active Filters* (2004), *Modern Electric, Hybrid Electric, and Fuel Cell Vehicles* (2nd ed, 2009), and *Integrated Power Electronic Converters and Digital Control* (2009). He was the Inaugural General Chair of the 2012 IEEE Transportation Electrification Conference and Expo (ITEC) and has chaired several IEEE and SAE conferences in the areas of vehicle power and propulsion. He was the Founding Editor-in-Chief of the IEEE TRANSACTIONS ON TRANSPORTATION ELECTRIFICATION, from 2014 to 2020. He is also the Editor of the *Handbook of Automotive Power Electronics and Motor Drives* (2005) and *Advanced Electric Drive Vehicles* (2014). He is the Co-Editor of the *Switched Reluctance Motor Drives* (2018).